Chinese Chemical Letters 35 (2024) 109511

Contents lists available at ScienceDirect

Chinese Chemical Letters

journal homepage: www.elsevier.com/locate/cclet

Flash nanocomplexation (FNC): A new microvolume mixing method for nanomedicine formulation

Keyang Li[a,b,c,1], Yanan Wang[a,b,1], Yatao Xu[a,b], Guohua Shi[a,b], Sixian Wei[a,b], Xue Zhang[a,b], Baomei Zhang[a,b], Qiang Jia[d], Huanhua Xu[e,*], Liangmin Yu[a,b], Jun Wu[f,*], Zhiyu He[a,b,*]

[a] Frontiers Science Center for Deep Ocean Multispheres and Earth Systems, Key Laboratory of Marine Chemistry Theory and Technology, Ministry of Education/Sanya Oceanographic Institution, Ocean University of China, Qingdao/Sanya 266100/572024, China
[b] College of Chemistry and Chemical Engineering, Ocean University of China, Qingdao 266003, China
[c] School of Materials Science and Engineering, Tsinghua University, Beijing 100084, China
[d] Guangzhou City Polytechnic, Guangzhou 510520, China
[e] National Key Laboratory for the Modernization of Classical and Famous Prescriptions of Chinese Medicine, Jiangxi University of Chinese Medicine, Nanchang 330004, China
[f] Division of Life Science, The Hong Kong University of Science and Technology, Hong Kong SAR 999077, China

ARTICLE INFO

Article history:
Received 13 November 2023
Revised 8 January 2024
Accepted 10 January 2024
Available online 12 January 2024

Keywords:
Nanoformulation
Nanoparticles
Self-assembly
Flash nanocomplexation
Kinetic control
Drug delivery

ABSTRACT

The application of nanotechnologies in formulation has significantly promoted the development of modern medical and pharmacological science, especially for nanoparticle-based drug delivery, bioimaging, and theranostics. The advancement of engineering particle design and fabrication is largely supported by a better understanding of how their apparent characteristics (*e.g.,* size and size distribution, surface morphology, colloidal stability, chemical composition) influence their *in vivo* biological performance, which raises an urgent need for practical nanoformulation methods. Based on turbulent flow mixing and the self-assembly of molecules in fluids, flash technologies emerged as effective bottom-up fabrication strategies for effective nanoformulation. Among the flash technology family, flash nanocomplexation (FNC) is considered a novel and promising candidate that can promote and optimize formulation processes in a precise spatiotemporal manner, thus obtaining excellent fabrication efficiency, reproducibility and expandability. This review presents an overview of recent advances in fabricating drug-delivery nanoparticles using FNC platforms. Firstly, brief introductions to the basic principles of FNC technology were carried out, followed by descriptions of turbulent microvolume mixers that have significantly promoted the efficiency of FNC-based fabrications. Applications of real formulation cases were then categorized according to the self-assembly-driven interactions (including electrostatic interaction, coordination interaction, hydrogen bonding and hydrophobic interaction) and discussed to reveal the progressiveness of fabricating nanoparticles and discuss how its flexibility will provide advances and replenish the philosophy of nanomedicine formulation. In the end, the commercial potential, current limitations, and prospects of FNC technology for nanoformulation will be summarized and discussed.

1. Introduction

The identification and application of biomedical nanoparticles or nanocomplexes to achieve efficient *in vivo* delivery of therapeutic agents are considered a recent breakthrough that has significantly aided in the treatment of a wide range of severe diseases (*e.g.,* metabolic disorders, cancers, cardiovascular diseases, and infectious diseases) [1–3]. However, the design of nanomedicine-based drug delivery platforms is vigorously contested due to the difficulties in producing desirable nanocarriers with controllable size, uniform morphology, high encapsulation efficiency, considerable colloidal stability, and other crucial properties [4–9]. Notably, a desirable nanocarrier fabricating method for encapsulating small molecular drugs, proteins, and nucleic acid therapeutics is supposed to provide both high reproducibility and feasibility in scale-up fabrication to ensure its competence in the broader scope of applications, as well as the potential for practical transition, which requires simplified and low-cost fabrication procedures [10–13].

* Corresponding authors.
E-mail addresses: huanhua323@jxutcm.edu.cn (H. Xu), junwuhkust@ust.hk (J. Wu), hezhiyu@ouc.edu.cn (Z. He).
[1] These authors contributed equally to this work.

https://doi.org/10.1016/j.cclet.2024.109511
1001-8417/

Iterations of formulation technologies appeared concurrently with the rapid development of chemistry, materials science and engineering [14–16]. The conversion from passive to active control of drug targeting is considered one of the milestones in this field, which has permanently changed formulation technology from the simple fabrication of traditional pharmaceuticals (tablets, powder, pills, injection fluid, *etc.*) to the precise design and fabrication of intelligent nanoscale drug carriers [17–23]. This giant leap also spurred the development of a large number of formulation technologies for the next generation, derived from conventional techniques. Currently, sophisticated formulation techniques, such as microfluidic mixing, hydrogel template methods, and colloidal evaporation induction, have become well-rounded in their contributions to the fabrication of drug carriers [24–28]. Moreover, with the rapid development of molecular biology, chemistry, and materials science, researchers have gained a deeper understanding of how bioactive nanomaterials and molecules will interact with the *in vivo* environment, which promotes a series of novel designs in nanomedical science. Therefore, combinations between biomanufacturing and advanced methodologies to achieve high scalability, reproducibility, and robustness of nanoformulations are urgently needed. Against this backdrop, flash technologies were developed with the core philosophy of achieving high-throughput and controlled nanocomplex or nanoparticle formulation in a turbulent environment [29,30]. As one of the most important branches of flash technologies, flash nanocomplexation (FNC) technology has grown rapidly. Various efficient nanoformulations based on FNC have demonstrated that, on account of non-covalent interactions and the flexibility to dominate phase-separation-induced nanocarrier fabrication, this advanced technology has the potential to be a future trend in rapid nanoformulation [31].

In this review, we will first discuss the origins and evolution of FNC technology before systematically elaborating on the underlying principles and concept of platform designation. According to the distinctions in self-assembly-driven interactions employed in the manufacturing process, research examples of FNC technology will be categorized into diverse topics. The formulation mechanisms under different driving forces, as well as how FNC technology promotes nanocarrier fabrication, will be summarized in detail. In addition, as a successful engineering example of this technology, the manufacturing of lipid nanoparticles for messenger RNA (mRNA) vaccines against corona virus disease 2019 (COVID-19) based on FNC technology will be introduced [32]. In the end, potential challenges and prospects for realizing the full potential of FNC nanoformulation in biomedicine will be discussed.

2. An overview of FNC: the next-generation microvolume mixing method

Before introducing the development of former formulation technologies and comparing them with FNC technology, it is necessary to identify factors that can be converted into technological optimization. Even though nanotechnology has been extensively studied and applied in the field of biomedicine and numerous studies have helped scientists gain a more systematic understanding of the interactions between nanoparticles and biological systems [33], further fundamental studies on bio-interfaces and nano-bio interactions are still urgently required to enable parameterization of the nanoformulation process by developing a specific philosophy of nanocarrier design (detailed discussions can be found in Supporting information) [34].

As a result of those constraints, traditional formulation methods have progressively diminished in favor of nanoformulation requirements. Compared with conventional administration methods, nano-formulated pharmaceuticals provide superior solubility, absorption, biocompatibility, and biodegradability. Moreover, scalability and controllability are also crucial for large-scale operations and future clinical transitions, which enable advanced pharmaceutical formulation technologies to become an intrinsic aspect of the drug delivery system [35]. Conventional batch-type formulation approaches, including bulk mixing, antisolvent precipitation, and colloidal evaporation induction, produce pharmaceuticals with poor particle size distribution, low particle colloid stability, and poor reproducibility. Due to their indisputable advantages of rapid mass and heat transfer, continuous microvolume methods have emerged in recent years as one of the key methodologies in the formulation of nanocarriers, with the great potential to overcome the limitations of conventional "bottom-up" approaches [36–38]. One of the essential processes in the reactor includes splitting the fluid into uniform elemental volumes with micro-scale turbulent flow and maintaining the uniform volumes at the molecular scale through molecular diffusion. Microvolume mixing refers to the process of blending uniform volumes at the molecular scales and microvolume continuous mass transfer permits the precision manipulation of micron-scale fluidic motions in preparation processes under immutable conditions, thereby facilitating high-throughput manufacturing [39–41].

Microfluidics appears as a technology that uses ultrafine pipelines to process and manipulate laminar liquids or droplets, which can be applied in nanoparticle fabrication procedures (Fig. S1A in Supporting information) [42]. A typical microfluidic device for nanoparticle fabrication consists of chemically resistant, low-dimensional (at least one-dimensional scales at $10–10^3$ μm) glass channels. A small volume of fluid ($1 \times 10^{-18}–1 \times 10^{-9}$ L) will participate in a series of nanoparticle processing stages (laminar stream or droplet) in a microfluidics-manipulated channel structure [43]. Microfluidic technology enables precise fluid control, designable microchannels of varying shapes, and a multi-channel programmed mixing process, which can act as a promising method for fabricating nanoparticles with uniform particle morphology and structure, uniform particle size distribution (with particle sizes ranging from 100 nm to 250 nm), and batch-to-batch quality control [44]. However, due to fluidic rate limitations (1 μm/s∼1 cm/s), the Reynolds number (*Re*) range of fluids in a microfluidic device is restricted to 10–200, exhibiting classical laminar behavior, which means diffusion dominates the mixture of components in the solution in the microfluidic process. As a result, the characteristic mixing time is extended to second levels (typically 1–5 s), which significantly limits the fabrication of small-size nanocomposite (with a particle size less than 50 nm). Meanwhile, the low volume of channels also restricts the production rate (approximately 20–100 mg/h) and makes the pipeline susceptible to clogging. Besides diminishing the quality of the final product, the necessity to periodically replace a clogged pipeline also increases expenses. All of the aforementioned problems constrained the application of microfluidic technology from prototype trials to industrial production [45–47].

According to the consensus on fluid properties, two distinct flow states can be distinguished: laminar flow and turbulent flow. When the flow velocity reaches a low state (*e.g.,* less than half of the central fluidic velocity in a tubular environment), the fluid flows in layers with no radial disturbance, which refers to the laminar flows. As the flow velocity gradually increases, the streamline of the fluid begins to become disturbed and enters a transitional state. When the flow velocity increases sufficiently, the formerly laminar flow will be disrupted, resulting in the emergence of turbulent flow. Although the regular movement of laminar flow results in a more controllable fluidic manner and less loss of pressure head, the low flow rate, high fluidic resistance, and lack of longitudinal fluid fracture hampered the output efficiency and production quality of laminar flow-based reactors significantly and promoted the emergence of turbulent mixing reactors.

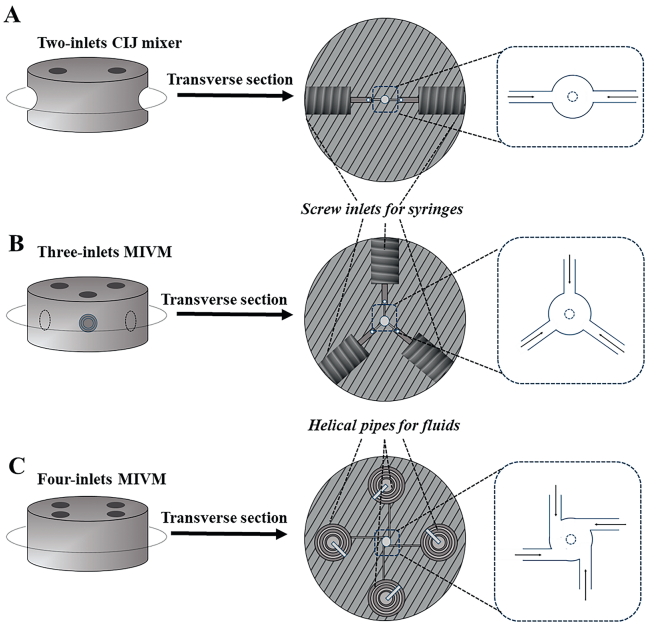

Fig. 1. Geometries of CIJM and MIVM and assorted syringes used in FNC processes. (A) The geometry of a CIJM with two opposing inlets leading to the mixing chamber. (B) The geometry of a MIVM with a triple-balanced arrangement of inlets leading to the mixing chamber. (C) The geometry of a MIVM with four inlets vertical to the plane containing helical pipes and a mixing chamber.

A typical turbulent mixing reactor comprises at least two stream inlets and a mixing chamber with a specific geometry structure [48,49], where solutions can be imported as jets and mixed with two or more jets (Figs. S1B and C in Supporting information). Stream injection creates a rapid burst of shear layers in fluids, allowing for high-degree mixing even in environments with a low *Re* ($Re = 600$) [50,51]. Confined impinging jet mixers (CIJM) and multiple inlet vortex mixers (MIVM) with the simplified geometries listed below were selected as the most commonly used devices to meet the mixing requirement (Fig. 1) [52–55]. Prud'homme *et al.* designed and developed the CIJM with two opposed cylindrical injector inlets that can provide an equal velocity impinge of solution and non-solvent liquid streams in the cylindrical mixing chamber, with this impinge driven by syringes and a high-pressure pump. The geometry of opposed jet inlets ensured that only fluidic streams with equal momentum were acceptable for CIJM-based flash manufacturing; otherwise, the high momentum stream would push the lower momentum stream back out of the chamber and jet inlet. To satisfy other fluidic fabrication demands for broader application, the development of dependable non-equal momentum mixers became an urgent task, which promoted the conception of MIVM. MIVM typically owns two or more jet inlets, and a comparison with the impinge fluidic structure in CIJM reveals that MIVM is more adaptable for generating multi-interactionally constructed ternary and quaternary nanoparticles with a higher production efficiency. To help understand the fluidic behaviors in MIVMs, Prud'homme *et al.* proposed a constant equation to explain the relationship between *Re* and mixing effectiveness (Eqs. 1–4) [54]:

$$X = \left(\frac{c}{Re-\alpha} + b\right) \tag{1}$$

where c, α, and b are constants; they also gave the experience equation for two and four inlets MIVM [54]:

$$X = \left(\frac{34.2}{Re-21.1}\right) \quad \text{two inlets MIVM} \tag{2}$$

and

$$X = \left(\frac{5.45}{Re-11} + 0.02\right) \quad \text{four inlets MIVM} \tag{3}$$

where effective *Re* can be described as [49]:

$$Re = \left[\sum_i \left(\frac{V_{\text{solution 1}}}{V_{\text{solution 2}}}\right)\left(\frac{V_i}{V_{\text{total}}}\right) Re_i^{2/3}\right]^{3/2} \tag{4}$$

where $V_{\text{solution 1}}$, $V_{\text{solution 2}}$, V_{total}, and V_i represent the total volumetric flow rate of the two different solution streams, the total volumetric rate of all streams, and the flow rate of stream i.

The internal geometry of the mixer and the ratio of streams are strongly related to the mixing efficiency. In a turbulent reactor, the mixing efficiency in the chamber will converge to a similar value regardless of the number of solution streams introduced [30,54]. CIJs and MIVMs can be considered fundamental devices for flash strategies, including flash nanoprecipitation (FNP), flash nanoemulsification, and FNC [55,56]. Since the inlets of mixers are typically combined with syringes and numerically controlled high-pressure pumps, the flow velocity, pressure head, and other associated parameters of streams can be precisely controlled, enabling flexibility to meet a variety of specific formulation requirements [29,57].

As a recently developed flash nanotechnology, FNC shares similarities with other flash techniques, especially FNP technology developed by Markwalter and Prud'homme (Fig. S1C) [55,58]. For both FNC and FNP, the formulation process (usually refers to a self-assembly process of the spontaneous formation of nanostructures by basic units including molecules, particles, microcrystals, and other nanostructures) is realized in a confined flow mixing environment, which allows the scalable fabrication of nanoparticles with tunable size, superior morphological uniformity, and high throughput capacitance [59]. To realize better responsiveness, most formulation processes are promoted by non-covalent interactions [60,61], and organized nanostructures (including liposomes, micelles, and core-shell structured nanoparticles) are designed to provide high *in vivo* stability, biocompatibility, and biodegradability to satisfy medical requirements [62,63]. It is worth noticing that FNP produces various types of nanoparticles through solvent supersaturation, whereas FNC usually produces nanoformulations *via* self-assembly driven by non-covalent interactions (including hydrogen bonding, electrostatic interactions, and hydrophilic-hydrophobic interactions) and has a high extendibility to couplet with other devices (including lyophilizers, homogenizers, and tangential flow filters) for high throughput formation and modification [64–67]. By using FNC technology, not only was the fabrication process simplified, but also an enhancement in the versatility of FNC-based nanofabrication could be earned, allowing higher availability for profound applications in therapeutic, diagnostic, biomarker monitoring, and fluorescence imaging fields [30,68]. Compared with other formulation methods, the unique design of mixers and simplified post-processing procedures have afforded FNC technology cost savings and improved quality management, along with higher scalability and reproducibility [69,70]. Moreover, compared with microfluidic technology, FNC exhibited several advantages that can be considered an optional choice for alternative or combinational technology with microfluidic: (1) Higher turbulent intensity. FNC technology, as a novel continuous microvolume mixing strategy, offers a turbulent mixing environment with higher *Re* (up to 2000, several times higher than microfluidic can offer). This enables rapid phase separation and aggregation for nanoformulations; (2) Precise controls the size, size distribution, and uniformity of the formulated nanoparticles. Due to the higher mixing efficiency, nanoparticles or nanocomposites formulated by FNC technology exhibited a narrower size distribution and higher uniformity. Moreover, FNC technology yielded superior results in formulating nanoparticles smaller than 50 nm due to its higher turbulence intensity, which effectively controlled particle size and dispersion by regulating solute nucleation and growth rates in the solution; (3) Higher component diversity of the formulated nanopar-

ticles. The special design of MIVM enables multiple solutions and components to be enrolled in nanoformulation to meet the requirements of high *in vivo* stability and multiple responsiveness proposed by advanced pharmaceutical designs [69]. According to the abovementioned advantages, FNC can be considered a novel technology for nanoformulation with higher feasibility and availability. In the following sections, the advantages of FNC technology will be highlighted by presenting research instances of successful nanoformulations based on FNC, and the mechanisms of formulations manipulated by various driving forces will also be introduced in detail.

3. Electrostatic self-assembly: fabricating nanoparticles with coulombic attractions *via* FNC technology

As a commonly employed non-covalent interaction in FNC-based formulations, electrostatic force (or so-called Coulombic force) has high efficiency in promoting the rapid complexation of macromolecules and oppositely charged substrates into nanoparticles. Natural and synthesized polycations, especially amino-rich cationic species (*e.g.,* chitosan, polyethyleneimine, and polyallylamine hydrochloride), are considered typically charged macromolecules that can be used in electrostatic-based formulations to fabricate nucleic acid-loaded nanoparticles due to the high biocompatibility, low immunogenicity, and low toxicity [71–74]. Moreover, the "proton sponge effect" demonstrated on amino-rich cationic species can protect the administered nanoparticles from lysosome internalization. When the pH of the lysosome environment decreases, amino-rich polycations can capture large amounts of protons. To reach charge and concentration equilibrium in the lysosome environment, Cl^- ions along with H_2O molecules in the cytoplasm will flow into the lysosome, inducing swelling and rupture of the lysosomes and allowing the nanoparticles to escape; thus, polycation-based nanoparticles usually exhibit higher transfection efficiency compared with other polymer-based nucleic acid carriers [72,75-77].

Researchers have found that the size, morphology, and surface properties of nanoparticles can be controlled during formulations by changing the pH, temperature, and solvent polarity. However, traditional laboratory preparation methods, including mechanical mixing of aqueous solutions, are incapable of achieving precise control of assembly kinetics, which results in the relatively larger size and wider size distribution, heterogeneous composition of the fabricated nanoparticles, and low batch-to-batch reproducibility in the formulation. Due to the aforementioned limits, the structures-properties relationship of the aforementioned nanoparticles has not been systematically studied and explained, which has remained a significant technical impediment to their clinical transition [78–81].

Linear polyethyleneimine (*l*PEI) is a widely used polycation with a high transfection ability. However, the reproducibility of *l*PEI-based nanoparticle fabrication mostly relies on the explicit control of kinetics [82–85]. As the diffusion rates of polycation and nucleic acid chains are faster than the electrostatic complexation rate, only when the mixing rate is faster than the assembly rate can the macromolecular chains be uniformly distributed before self-assembly to achieve high batch-to-batch reproducibility. FNC technology has been proven to be a viable strategy as the turbulent environment enables precise dynamic control for polycation-nucleic acid complexation, which also assists researchers in gaining a deeper understanding of the complicated formulation. Hu *et al.* used a 2-inlet CIJM-based FNC device to manufacture *l*PEI/DNA nanoparticles loaded with different types of plasmid DNA (pDNA) at different payloads. Turbulence in the CIJM chamber induced by two opposed jet collisions promotes higher mixing efficiency of fluids compared with traditional mixing strategies including vortexing and pipetting (Fig. 2A). Moreover, the authors analyzed the two-step *l*PEI/DNA nanoparticle assembly model in turbulent mixing conditions by investigating the batch conditions by computational fluidic dynamic (CFD) simulation and concluded that binding and charge neutralization processes will occur before chain condensation and particle association (Fig. 2B). The relationship between particle size and preparation parameters was subsequently demonstrated using transmission electron microscopy (TEM) images and size distribution analysis. Briefly, a higher injecting flow rate $\boldsymbol{Q}$ will lead to a shortened characteristic mixing time $\boldsymbol{\tau_M}$ of the species, along with a smaller particle size and a narrower size distribution of the fabricated nanoparticles (Figs. 2C and D). As the constitution and nitrogen/phosphorus (N/P) ratios of *l*PEI/DNA nanoparticles can be precisely controlled in an FNC device by changing the fluidic conditions, the *in vivo* and *in vitro* transfection efficiency of nanoparticles (N/P ratios ranging from 3 to 6) prepared under both a low flow rate ($\boldsymbol{Q}=5$ mL/min) and a fast flow rate ($\boldsymbol{Q}=20$ mL/min) are tested and compared, and the results indicate that nanoparticles prepared under a faster flow rate have better reproducibility and transfection efficiency, especially in situations with a lower N/P value (N/P ratio = 3 and 4) (Figs. 2E and F). Besides, scaled-up production of *l*PEI/DNA nanoparticles and long-term storage stability was realized by precisely controlling the characteristic mixing time and velocity. Nanoparticles exhibited durable characteristics (including stable ζ potential, particle size, and size distribution) even after being lyophilized at $-20\,^{\circ}C$ for 9 months. The results of luciferase expression show that lyophilized and reconstituted nanoparticles have an *in vitro* transfection efficiency that is comparable to that of fresh nanoparticles ($P=0.19$, statistically insignificant difference) (Fig. 2G). The development of FNC-based experiences and nanoparticle formulation models under the guidance of CFD exhibited high instructive significance for future works based on *l*PEI-based nanoparticles [82].

Lentivirus (LVV)-based gene therapy is an effective treatment option for a variety of chronic diseases, and transient transfection in production cell lines has become one of the most widespread methods for producing LVV carriers. However, the batch-mode mixing process in formulating LVV carriers is hard to control, making uniform formulation during the mixing process impossible to achieve. Thus, there is an imperative need for a platform with high scalability for achieving consistent yields of LVVs. According to the above-mentioned work [82], the transfection efficiency of LVVs is strongly related to nanoparticle size [86], thus Hu *et al.* designed an FNC-coupled step-by-step engineering approach to fabricate PEI/DNA nanoparticles in a consistent and highly extensible manner by shifting surface charge and changing the ionic strength of the solution (Fig. 3A). Before establishing the fabrication platform, the authors used *in-situ* dynamic light scattering (DLS) monitoring to investigate the relationship between particle size and incubation time. As the pre-experiment demonstrated that the growth rate of particle size can be presented predictably and the highest transfection efficiency was realized when particle size reached 400–500 nm, the authors were motivated to apply the FNC technology to accomplish the preparation of sub-micrometer DNA/PEI particles (Figs. 3B and C). Though traditional single-mixer-based FNC technology can only accomplish discrete particle size control below 100 nm, a block-building assembly strategy involving three FNC mixers is established (Fig. 3D). As the protonation degree of imine nitrogen atoms in PEI can be controlled and regulated by analyzing and changing pH value, individual small nanoparticles (size: 50–60 nm) were prepared at pH ~3.0, and as the pH value increased to 7.0, the deprotonation process of nitrogen atoms decreased the surficial potential value and thus promoted particle association, thus inducing particle size grew (size: 300–1000 nm). The turbulent environment created by CIJ mixers enabled these abovementioned processes to be accomplished at high flow rates while op-

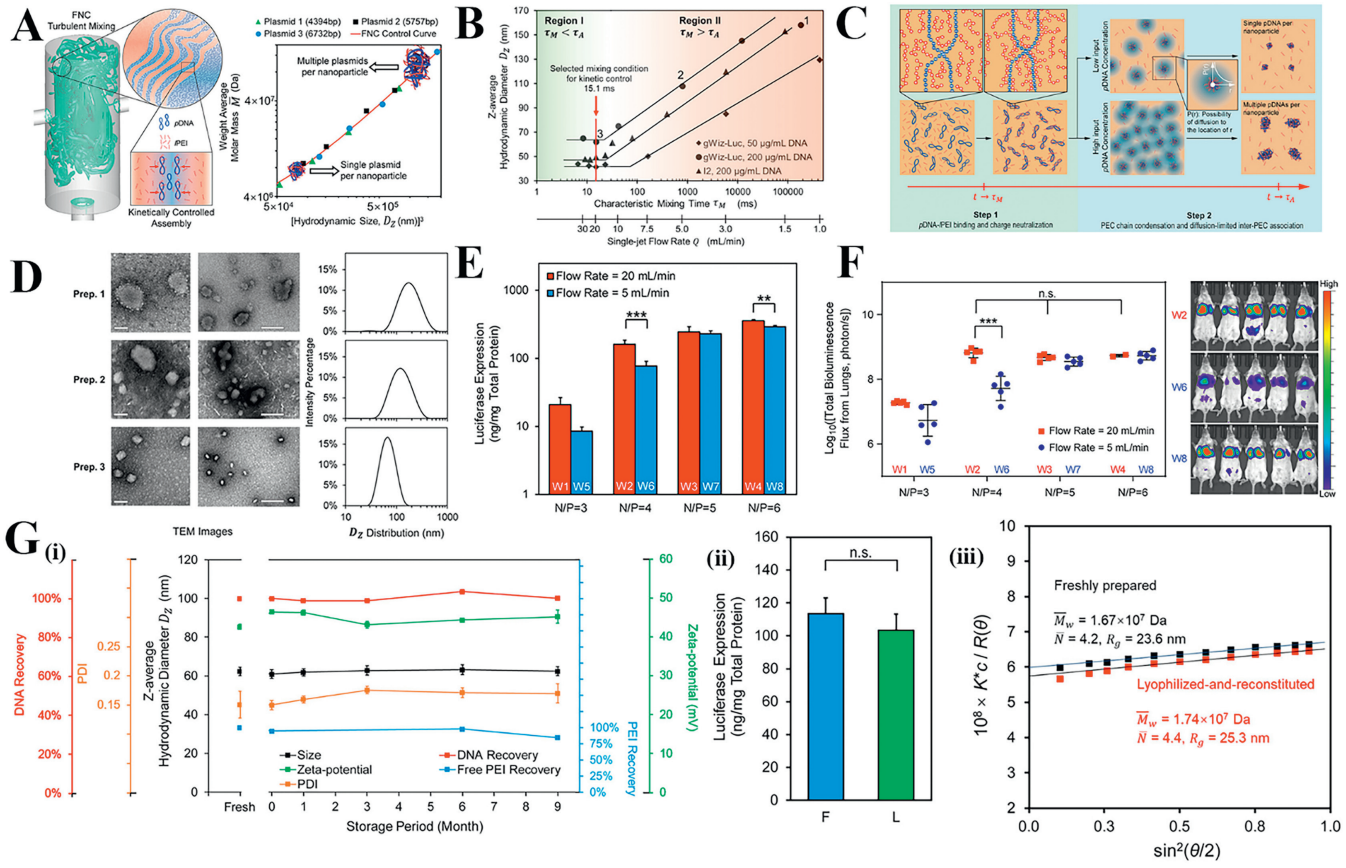

Fig. 2. (A) Turbulent mixing in a confined impinging jet (CIJ) microchamber and the FNC control curve fitting with single or multiple-plasmid-loaded nanoparticles. (B) A proposed two-step mechanism for pDNA/*l*PEI nanoparticle self-assembly in a turbulent environment. (C) The effect produced by $\boldsymbol{\tau_m}$ and flow rate $\boldsymbol{Q}$ on the average nanoparticle size. (D) TEM images and size distribution of the three sets of nanoparticles prepared at $\boldsymbol{Q}$ = 1.25 mL/min, $\boldsymbol{\tau_M}$ = 1.8 × 10^5 ms (prep 1), $\boldsymbol{Q}$ = 5 mL/min, $\boldsymbol{\tau_M}$ = 790 ms (prep 2), and $\boldsymbol{Q}$ = 20 mL/min, $\boldsymbol{\tau_M}$ = 15 ms (prep 3). (E) *In vitro* transfection efficiencies of nanoparticles (with different N/P values, prepared under flow rates of 20 mL/min and 5 mL/min) in the PC3 cancer cell line (F) *In vivo* transfection efficiency in the lung in healthy BALB/c mice at 12 h post *i.v.* injection of nanoparticles (W1-W8) containing 40 μg of gWiz-Luc plasmid per mouse (left) and representative bioluminescence images of groups with significant differences in transgene expression (right). (G) Scale-up production of off-the-shelf pDNA/*l*PEI nanoparticles and the long-term storage stability. (i) *In vitro* transfection efficiency comparison between freshly prepared nanoparticles and lyophilized-and-reconstituted nanoparticles; (ii) particle size and ζ-potential characteristics upon reconstitution of lyophilized nanoparticles after 0, 1, 3, 6, and 9 months of storage at −20 °C; (iii) Debye plot analysis comparations between freshly prepared and lyophilized-and-reconstituted nanoparticles. Copied with permission [82]. Copyright 2019, American Chemical Society.

timizing the fluidic environment for large-scale operation simultaneously. The production scale can be expanded up to 100 mL as the mixing process is adjusted to the tailored assembly kinetics. In the final step, when the nanoparticles were applied in bioreactors to produce LVVs, the infectious titers of microparticles with sizes of 400 nm predominated, implying that they may enhance the expression for advanced LVV production and assembly processes (Fig. 3E). This new FNC-based fabrication method for LVVs has excellent translational potential for the production of nucleic acid carriers [86].

Polyethylene glycol (PEG) grafting is a widely used strategy to enhance the colloidal stability of nanoparticles by decorating the surface of polycation carriers. Although researchers have investigated how the length of PEG chains and the grafting density of PEGylation can affect the physicochemical properties and transfection efficiency of nanoparticles, a systematic understanding of the effects of PEG terminal groups is still needed [30]. Since molecular dynamic simulation demonstrated that nanoparticles with intermediate chain length (containing 4–6 carbon atoms) have the highest transfection efficiency, Ke *et al.* conducted an integrated experiment to investigate how the properties of grafted polymeric terminal groups influence the interactions between polycation-based nanoparticles and cell membranes. In pulmonary cells, PEGylated nanoparticles with a PEG grafting ratio of 0.5% and amino or amino acid terminal groups demonstrated the highest levels of transgene expression. In this work, to satisfy the requirement of the large-scale integrated experiment, the FNC platform was applied to simplify the continuous fabrication of series PEG-PEI/mRNA nanoparticles and their surface decoration processes. Moreover, the high batch-to-batch reproducibility of the FNC platform allowed the fabricated nanoparticles to be stored in a lyophilized state at −20 °C for more than 4 months with no detectable variations in particle size or transfection activity after reconstitution [87,88].

Nanoformulations based on electrostatic interactions for protein and peptide delivery had become another practical strategy, as the charged residues promoted the complexation of protein and peptide with oppositely charged materials [89,90]. Although curative peptides and proteins have been recognized as attractive therapeutical agents in drug delivery science in recent decades and a large number of protein/peptide formulations have been approved by the Food and Drug Administration (FDA) [91], the low oral bioavailability caused by the hostile gastrointestinal barriers has severely impeded their clinical transition. Currently, only a few oral nanoformulations of peptide/protein are commercially available (*e.g.,* ciclosporin A, semaglutide, octreotide, voclosporin) [92–95]. Moreover, potential shortcomings such as protein denaturation, spontaneous initial burst release, and uncontrollable release

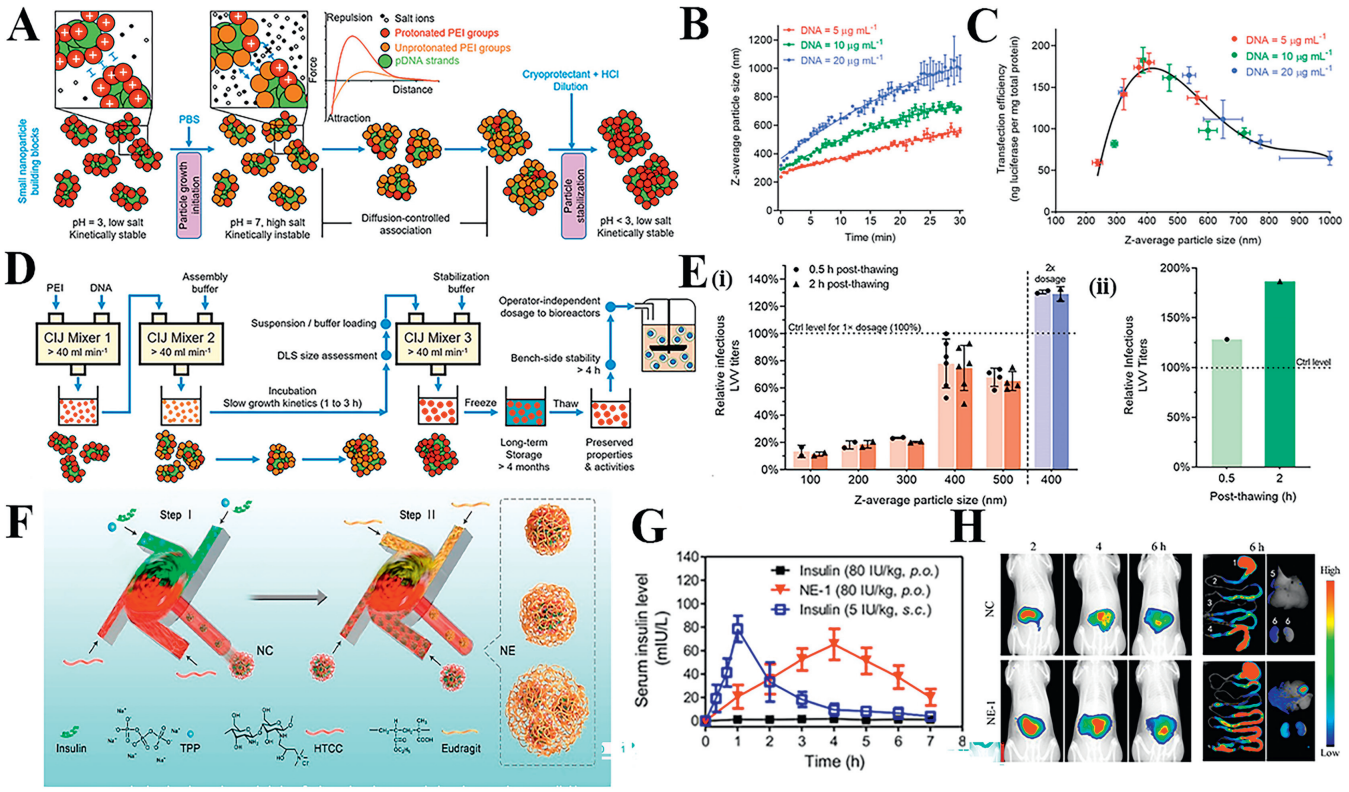

Fig. 3. (A) Schematic of the stepwise preparation of PEI/DNA nano/micro particles for LVVs productions. (B) Relationship between particle size and incubation time for particles loading different amounts of DNA. (C) Transfection efficiencies are valued by different quotas of stabilized particles with controlled sizes ranging from 60 nm to 1000 nm. (D) Schematic of the large-scale production process with two CIJ mixers. (E) Transfection evaluation of pDNA/PEI particle size on the infectious titers. The control level represents the optimal results from the standardized in-house procedures to prepare pDNA/PEI particles manually immediately before the transfection experiments. (i) Higher relative infectious LVVs titers. Achieved by 400 nm particles; (ii) after expanding the production scale, 400 nm particles present superior infectious titers in the purified LVV preparation (128% and 187% over the control level). Copied with permission [86]. Copyright 2021, American Chemical Society. (F) Schematic graph of fabricating NC-in-Eudragit composite nanoparticles (NE) *via* a two-step FNC process. (G) Changes of serum insulin level after administration of insulin (80 IU/kg, *p.o.* and 5 IU/kg, *s.c.*) and NE-1 (80 IU/kg, *p.o.*). (H) Whole-body imaging and ex vivo main organ imaging of the rats after oral administration of NC and NE-1 (Insulin labeled with Cy-7, 80 IU/kg, 6 h after administration; 1. stomach; 2. duodenum; 3. jejunum; 4. ileum; 5. liver; 6. kidney). Copied with permission [103]. Copyright 2018, American Chemical Society.

kinetics remain concerns [96–99]. The invention and development of FNC technology appear to break the above-mentioned deadlocks since the feasibility of the FNC devices to fabricate homogeneous surface coatings on nanocarriers, which is essential for acceptable bioavailability and biocompatibility when protein and peptide formulations are employed.

Insulin is one of the most widely used therapeutic agents for type I diabetes, but its administration is limited due to its poor gastrointestinal stability. Traditional hypodermic injections cause intolerable suffering for patients both physiologically and psychologically, while also increasing the risk of wound infection. Researchers have exerted significant effort to realize the goal of effective oral insulin delivery, and the most important procedure in dealing with this difficulty is the fabrication of nanocarriers to protect this delicate protein from gastrointestinal digestion and pass through the intestinal mucosal barrier, thus promoting protein absorption into the circulation system [100–102]. Stepwise-FNC provides a new strategy for the flexible fabrication of nanoparticles with a core-shell structure. With intestinal-lysis materials serving as the shell to protect the protein against pepsin digestion and the acerbic environment, a series of innovations have emerged. For example, Sun *et al.* developed a practical insulin oral delivery strategy in which a two-step FNC-based fabrication procedure was the key to achieving a high protective effect from the acidic stomach environment [103]. First, the insulin-loaded *N*-(2-hydroxypropyl)-3-trimethyl ammonium chloride modified chitosan (HTCC)/sodium tripolyphosphate (TPP) nanocomplex was generated as the core of nanoplatforms by rapidly and efficiently confined mixing of insulin/TPP solution and HTCC solution in the chamber of a four-inlets MIVM device. Then the nanocomplexes were encapsulated within intestinal-lysis material Enteric Eudragit L100-55 *via* another FNC mixer serving as the secondary encapsulating device, where the core-shell-structured nanoparticles NE-1 were fabricated (Fig. 3F). *In vivo* studies revealed that the NE-1 formulation exhibited better insulin pharmacokinetic curves for restraining burst release along with a controlled release pattern compared with the other two insulin administration routes (insulin 80 IU/kg, *p.o.*, and 5 IU/kg, *s.c.*) (Fig. 3G). *In vivo* biodistribution and in situ oral absorption of NE-1 were also observed with insulin dyed by Cy7 (a commonly used near-infrared fluorescent group for labeling proteins and peptides). In comparison to the biodistribution of NC, the NE-1-administered group showed stronger fluorescence intensity, particularly in the ileum segment of the small intestine, demonstrating that the encapsulation ability of enteric Eudragit protected the denaturation and acidic degradation of the stomach environment (Fig. 3H). Moreover, tissue observation of the administered ileum segment (insulin labeled with RITP dye) was explored, and the NE-1-administered group showed a stronger fluorescence signal compared with the NC group, proving that better absorption and biodistribution can be achieved through NE-1-based oral dosing. All of the findings in this work confirmed that the optimized intestinal-lysis formulation has a high potential for oral delivery of insulin and other peptide and protein agents. As a versatile and robust formulation platform, FNC created high-turbulence mixing for components to form stable nanocomplexes for the encapsulation of insulin with high throughput and

versatility. Moreover, the FNC-based formulation process executed in aqueous solutions avoids the aggregation or precipitation of nanoparticles induced by the phase separation of organic solvents and water. These above-mentioned advantages of FNC technology have significantly expanded the applications of FNC-based oral delivery nanoformulations [103].

Gating modifier toxins (GMTs) are newly developed therapeutical agents for type II diabetes caused by hyperglycemia, but their applications are severely limited by their high acute toxicity and rapid *in vitro* clearance. GMTs, on the other hand, exhibit highly positive ζ-potential in aqueous solutions, which allows the development of an electrostatic interaction-based nanoparticle system for safe and effective delivery. Gui *et al.* used the FNC technology to fabricate long-lasting nanoplatforms based on the electrostatic interactions between melittin (a commonly used GMT model) and dextran sulfate (DS), a negatively charged natural polymer [104]. In this case, FNC technology was successfully employed, and the flexibility of MIVM-based mixing modes resulted in nearly 100% melittin encapsulation efficiency and a high payload capacity ($\sim$30%). The *in vitro* drug release process was prolonged, and the release profiles were formulated to be tunable. Comparing with the melittin single intraperitoneal (*i.p.*) T2D mouse model, the 8-day survival rate of nanoparticle-injected T2D mouse models increased from 60% to 100%. The high *in vitro* stability and sustained release behavior provided by GMTs-encapsulated nanoparticles have broadened the applications of GMTs as effective therapeutic agents, as well as other peptides with non-negligible but evadable toxicity [104].

4. Multi-force-promoted self-assembly: applying FNC technology in metal-ligand coordination and hydrogen bonding enrolled nanoformulation systems

Coupling transition-metal ions as coordination centers to fabricate metal-ligand coordination networks as drug delivery platforms have become increasingly popular due to the variety of ligands and central ions enhancing the diversity of interactions in nanostructures [105]. Meanwhile, hydrogen bonding is usually accompanied by metal-ligand coordination or acts as a substitute strategy, as hydroxy groups and amino groups, the initiators of hydrogen bonding, are abundant in natural/synthesized polymers [106]. Compared with traditional pharmaceutical preparations, by incorporating other interactions such as covalent bonding, van der Waals force, and π-π stacking, the multi-force fabricated nanocarriers could be considered valid drug delivery platforms and extremely suitable for loading small molecular drugs and oligopeptides, as their molecular structures are usually under thorough analysis [107]. Different from the nucleus acid and protein agents, small organic molecules and oligopeptides cost less, along with acceptable tissue and cell selectivity. Moreover, lower molecular mass and a relatively simple molecular structure determined that these agents possess less than no antigenic determinants [108–110]. However, the application of small molecular agents is seriously hampered by various limits, like poor permeability through biological barriers, low bioavailability and biodegradability. Also, the complexity of the *in vivo* environment restricts their usage; pH value, temperature, interference of soluble inorganic salt, and other factors require further modulation in the design of small-molecule-loaded nanocarriers [111]. Metal-ligand coordination and other non-covalent assembly-driven forces are sensitive to changes in the microenvironment, which means stimulation-responsive manners can be achieved [105,112]. The self-assembly-driven interactions will not only stabilize the nanostructure of particles but also modify the drug release in a sustained manner when the circulation system brings the nanoparticles to target cells, tissues or organs [113,114]. FNC, as a microvolume continuous mixing technology offering the advantages of higher mixing efficiency for multiple reaction components, has proposed new strategies for fabricating multi-force-promoted nanoparticles [115].

As one of the standard therapeutics for Parkinson's disease (PD), levodopa (L-DOPA), however, can be easily decarboxylated to dopamine by decarboxylase in the liver for the first time in absorption, and it is hard for dopamine to pass through the blood-brain barrier, which means only less than 1% of L-DOPA can be transported to the brain [116,117]. As L-DOPA contains a rich abundance of hydrogen bond donors and acceptors, components with plentiful hydroxyl groups for hydrogen bond formation have high potential for caging L-DOPA to form nanocarriers with enhanced loading capacity and inhibition on burst release. The aqueous formulation environment also allowed the use of FNC technology for the continuous fabrication of uniform nanocarriers. Therefore, to produce quality-guaranteed L-DOPA-loaded nanoparticles for high-efficiency delivery, Nie *et al.* designed an FNC-based formulation strategy for the fabrication of tannic acid/polyvinyl alcohol/L-DOPA (TA/PVA/L-DOPA) nanoparticles *via* hydrogen bonding and π-π stacking. (Fig. 4A). Fourier transform infrared spectroscopy (FT-IR) results on the reagent and nanoparticles proved the formation of hydrogen bonding between the carbonyl group on L-DOPA and TA/PVA as a board absorption peak of the carbonyl group appeared along with the red-shifted absorption peak corresponding to the hydroxyl groups in TA and PVA (Fig. 4B). The optimized result of fabricating was sifted by changing the concentration and pH value of PVA, L-DOPA concentration, and volumetric flow rate (Fig. 4C). To pass through the blood-brain barrier, size distribution control is essential, as smaller nanoparticles are less likely to be trapped, which enables their higher delivery efficiency. The authors chose 0.2 mg/mL PVA, a weakly acidic environment (maintained by dissolving dissolved PVA in 100 mmol/L *N*-2–hydroxy ethylpiperazine-*N*′−2-ethanesulfonic acid buffer), and a relatively higher flow rate for further optimization [118]. The batch of nanoparticles with an average size of around 50 nm according to the TEM image was selected for further *in vivo* environments as it was predicted to have the best permeability to the blood-brain barrier (Fig. 4D). Results of *in vivo* experiments exhibited that TA/PVA/L-DOPA nanoparticles achieved effective biodistribution in target organs while also ameliorating movement disorders and striatal dysfunction. A roller test on the model group proved that TA/PVA/L-DOPA nanoparticles can alleviate damage to motor coordination and fatigue in the nervous system (Fig. 4E). Moreover, the acute toxicity of L-DOPA was also restricted by nanoparticle encapsulation, which proved that this FNC-based nanoformulation has a high potential for future clinical translation toward PD treatment [118]. The turbulent environment offered by FNC technology enabled the intensive mixing of all the components in the ternary nanoparticle system for multi-interaction enrolled self-assembly in a continuous manner, and the flexibility of the FNC system provided convenience for changing the fluidic condition to determine and optimize the best formulation condition and also secured batch-to-batch reproducibility for establishing reliability from a large number of orthogonal experiments. Moreover, in this case, FNC technology presents high robustness, consistently yield homogeneous nanoparticles regardless of the changes in flow rates, concentrations, and other formulation parameters.

Another multi-force-driven nanocomplex formulation realized on the FNC platform was carried out by Le *et al.,* which was designed against acute lung inflammation [119]. The authors chose a series of polyphenols (*e.g.,* tannic acid, procyanidin and epigallocatechin gallate) along with D-α-tocopheryl polyethylene glycol 1000 succinate (TPGS) to form the nanocomplexes, as TPGS exhibits potential for neutralizing intracellular ROS, which can aggravate dysregulated inflammation. Moreover, the hydrophilic PEG polar head in TPGS molecules allowed the formation of hydrogen

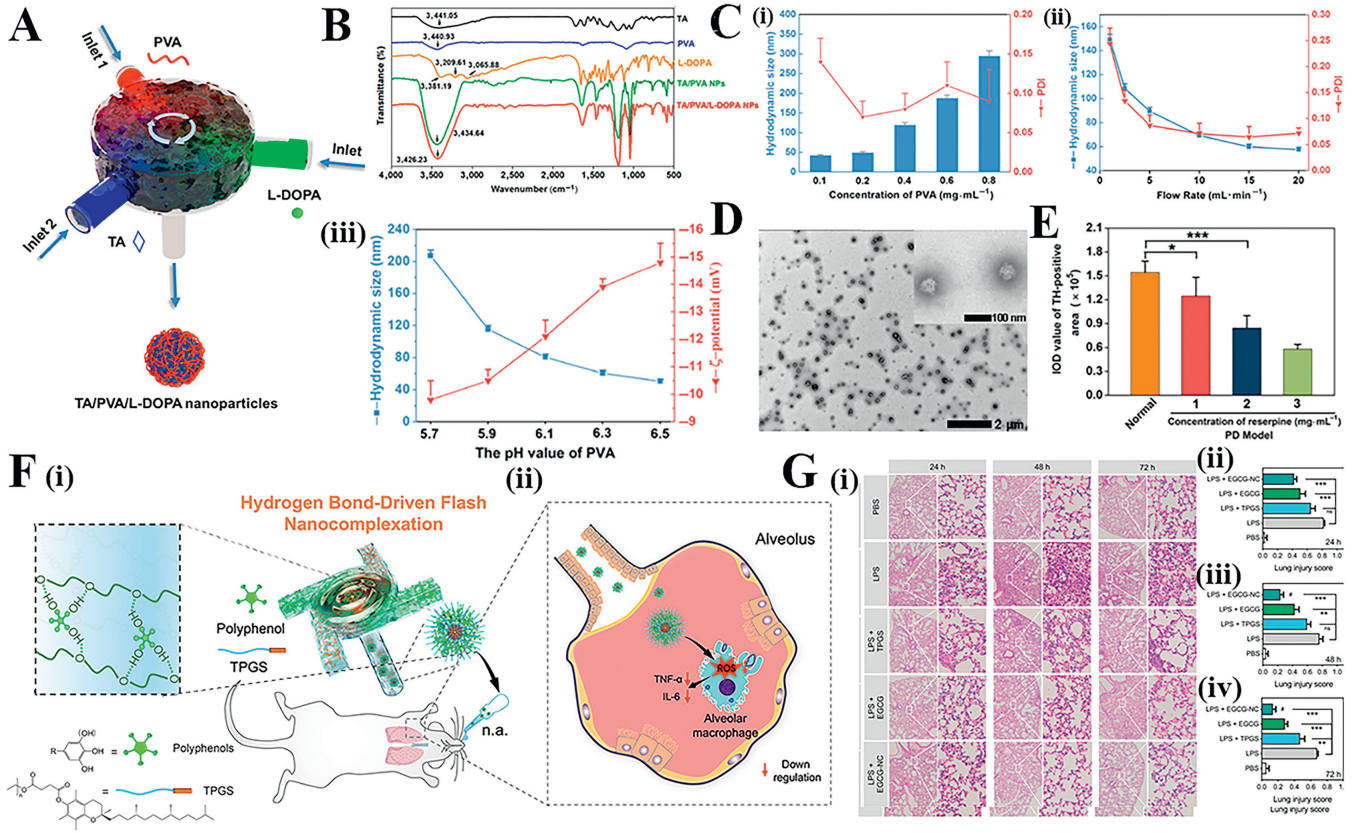

Fig. 4. (A) TA/PVA/L-DOPA nanoparticle preparation *via* the FNC method. (B) FT-IR characterization of reagents and empty and drug-loaded nanoparticles. (C) Characterization of TA/PVA/L-DOPA nanoparticles. (i) Influence of PVA concentration on nanoparticle size and PDI in FNC preparation; (ii) influence of flow rate on nanoparticle size and PDI; (iii) influence of pH value of PVA solution on nanoparticle size and ζ-potential. (D) TEM graphs of nanoparticles with diameters less than 100 nm. (E) Roller test results of groups treated by TA/PVA/L-DOPA nanoparticles with different administration forms after 2 h. Copied with permission [118]. Copyright 2021, Springer Nature. (F) Nanocomplexes comprising polyphenols and TPGS produced through an FNC process for alleviation of acute lung injury. (i) The assembly mechanism of polyphenol/TPGS nanocomplexes through hydrogen bonding; (ii) a possible mechanism of TPGS down-regulating the ROS level in the alveolus to alleviate acute lung injury (ALI). (G) (i) Hematoxylin and eosin (H&E)-stained images of lung tissue sections from the normal mice (PBS), lipopolysaccharide-induced model mice (LPS), and the model mice treated with TPGS (LPS + TPGS), epigallocatechin gallate (LPS + EGCG), or EGCG/TPGS nanocomplex (LPS + EGCG-NC), respectively (×200). Lung injury score at posttreatment of 24 h (ii), 48 h (iii), or 72 h (iv). Copied with permission [119]. Copyright 2020, American Chemical Society.

bonds with polyphenol, which was considered one of the driving interactions in complexation (Fig. 4F). The dynamic light scattering (DLS) results on hydrated particle size and TEM images exhibited that the nanocomplex has high morphology homogeneity and relatively narrow size distribution. As the molecular structure dominates the intermolecular interactions to form uniform nanocomplexes, by adapting FNC technology for verification of repeatability, the authors found that only polyphenols containing over 8 phenolic hydroxyl groups can participate in forming nanocomplexes with secured colloidal stability. Meanwhile, the excellent *in vivo* antioxidation and antiinflammation ability of this nanocomplex confirmed that the polyphenol-dominated complexion is effective enough to be a universal strategy for anti-acute-inflammation therapeutic carrier formulation (Fig. 4G) [119].

Compared with synthesized small-molecule drugs, short-peptide therapeutics gradually exhibit their potential for serving as new-generation therapeutics with higher bioactivity and therapeutic efficiency. The amino acid residues play important roles in fabricating peptide-loaded nanoparticles. Hydroxyl, azyl, thiol and carbonyl groups can act as excellent hydrogen bonding donors and acceptors; aromatic residues (*e.g.,* indole residues served by tryptophan, benzyl residues served by phenylalanine and imidazole residues served by histidine) will participate in π-π stacking interactions; nitrogen and oxygen atom-containing residues like tetrahydropyrrole served by proline will act as ligands in coordination crosslinks. Recently, multi-force-promoted peptide-encapsulating nanoparticles have been gaining more and more attention. Liu *et al.* reported a coordination-driven FNC strategy to realize a reproducible fabrication of doxorubicin-based metal-phenolic nanoparticles (DITH) with a hyaluronic acid surface layer, where Fe^{3+} ions act as the coordination center in this process [120]. A four-inlet MIVM was employed, and characterizations towards concentration and size distribution of nanoparticles exhibited that tannic acid (TA) and dopamine-grafted hyaluronic acid (HAd) play critical roles in nanoparticle fabrication, as particles without TA or HAd will easily aggregate at room temperature. The prepared DITH has impressive long-term colloidal stability even after storage at 4 °C for 2 months and excellent biostability in particle size and distribution, which can be attributed to the existence of a hydrophilic HA surface and a Fe^{3+}-TA crosslinked coordination network [120].

Achieving precise kinetic control in a multi-force enrolled nanoparticle assembly system is considered a tough task due to the difference in kinetic rates of competitive reactions. Owning the ability to facilitate the efficient mixing of multiple components in fluids, FNC technology exhibits huge potential for controlling and optimizing the formulation processes by balancing the dynamic behaviors of fluids [121]. Wang *et al.* designed a ternary system with phytic acid (PA) and Fe^{3+} to realize sustained delivery of lixisenatide (Lix). As multiple interactions, including electrostatic interactions and coordination reactions, were enrolled, the rate difference between the slow reaction (formation of PA/Lix phytate-

peptide complexes, promoted by electrostatic interaction between the anionic phosphate groups of PA and cationic groups of Lix, *via* thermodynamic control) and the fast reaction (formation of PA/Fe^{3+} chelates, promoted by coordination interactions, *via* kinetic control) required the mixing kinetics of three components to reach the dynamic equilibrium of the three competitive combinations while avoiding the formation of heterocomplex particles. Here, the researchers applied the FNC technology to achieve a uniform distribution of multiple components. The adapted CIJ enabled better control of assembly kinetics. The flexibility of FNC technology to adjust mixing conditions, including flow rate, concentration, mass ratio, *etc.,* enabled the nanoparticle-producing processes to be highly uniform and scalability manner. The produced ternary nanoparticles have a relatively small particle size (∼50 nm) and uniform composition (polydispersity index (PDI) ∼0.12), as well as an encapsulation efficiency (∼100%). With a sustained Lix release period over 8 days, upon only one single injection (600 μg/kg), the blood glucose level (BGL) from 30 mmol/L back to lower than 10 mmol/L in the T2D mouse model, which refers to a high-efficiency blood controlling procedure, can be achieved in a single administration. The self-assembly-driven forces will not only stabilize the nanostructure of particles but also induce drug release in a sustained manner when the circulation system brings the nanoparticles to target cells, tissues or organs [121].

Liraglutide (Lira), as an approved GLP-1 receptor antagonist for T2D treatment, has exhibited excellent curative effects in lowering blood glucose levels and improving cardiovascular function. To prolong the short half-life and expand the application for Lira, based on the peptide-polyphenol-ion hydrogen bonding and polyphenol-ion coordination interaction, He *et al.* developed a Lira/tannic acid (TA)/Al^{3+} ternary nanoparticle formulation system to achieve sustained release of Lira [122]. As the phenol groups of tannic acid will partially ionize under physiological pH value, inducing the weakening of hydrogen bonding to release peptide, a sustained release manner of Lira had been enabled. Al^{3+} ions coupled in this system not only acted as the coordination central ions but also quenched the surplus phenol groups to inhibit the overgrowth of the TA/Lira complex. Adapting the FNC platform enabled the preparation processes can be optimized for enabling a higher encapsulation rate and better drug release profile, as well as enhancing the size distribution, morphological uniformity, and colloidal stability (Fig. 5A). By shifting the preparation conditions, a series of nanoparticles are fabricated and in the *in vivo* experiments, comparing with free Lira administration, administrating the ternary nanoparticle formulations led to better long-time (168 h) BGL control, which means a gradual release of Lira-mediated by nanoparticles had significantly enhanced its persistence in the blood circulation system. (Fig. 5B). Fluorescence imaging for biodistribution of Lira proved the valid *in vivo* sustained release of Lira can persist for over 6 days. Besides, the fluorescence intensity evaluations of blood samples proved that compared with free Lira administration, the burst release in the initial stage had been suppressed in nanoparticle administration groups (Fig. 5C). Assisted with the scalable, highly reproducible FNC technology, these long-acting peptide release systems exhibit excellent preclinical performance for T2D treatments [122].

Cyclic diadenosine monophosphate (c-di-AMP) is considered a promising agonist of the cGAS/stimulator of interferon genes (STING) pathway for immunotherapy against a variety of cancer. However, due to the immunosuppressive microenvironment of the tumor, immunotherapy or immunotherapy-cooperated combinational therapies can hardly antagonize large tumors. As metal-cyclic dinucleotide nanomodulators have shown potential for improving the inflammatory or tumor microenvironment, Wang *et al.* designed manganese(II)-tannic acid-based nanoparticles (TMA-NPs) to encapsulate c-di-AMP for immunotherapy and radiotherapy synergic treatment [123]. To achieve high efficiency in nanoformulation, the synthesis of TMA-NPs was realized by FNC technology through a homogeneous mixture in a CIJ device. FNC technology enables uniform dispersion and mixing of Mn^{2+} ions and c-di-AMP with tannic acid in the mixing chamber of CIJ under turbulent conditions, resulting in the formation of TMA-NPs through the metal-polyphenol network. The high uniformity in morphology (spherical shape) and size distribution (25.7 nm) of the TMA-NPs, along with the excellent loading efficiency of Mn^{2+} and c-di-AMP (81.3% and 85.4%, respectively), can be attributed to the high homogeneity of fluid mixing under the turbulent environment brought by FNC technology, as observed under TEM. According to the magnetic resonance imaging (MRI) result, TMA-NPs can markedly alleviate hypoxia in the large tumor with the oxygenation of Mn^{2+} ions, resulting in ROS overproduction and DNA damage by X-ray irradiation to release c-di-AMP and Mn^{2+} from the nanoparticles along with DNA fragments to enhance STING activation in large tumors. This research exhibited the high potential and feasibility of FNC technology to formulate multi-functional nanocarriers for complicated syngeneic therapy for tumors and other major medical cases [123].

5. Hydrophobic interaction-based self-assembly: fabricating lipid/amphiphilic polymer-based nanoparticles *via* FNC technology

Mediated by oil-water segregation, hydrophobic interactions play an important role in amphiphilic macromolecule self-assembly. Lipid-based nanoparticles are the most widely-applicated nanocarriers fabricated by hydrophobic forces [124]. Ionizable lipids, phospholipids, and cholesterol are commonly used components for lipid-based nanoparticle fabrication, but they play different roles. Ionizable lipids can form complexes with negatively charged molecules; cholesterol and phospholipids can offer mechanical strength for nanoparticles by acting as skeleton components; and the circulation stability of nanoparticles can be enhanced by PEG-grafted lipids [125–129]. Depending on their constitutional differences, hydrophobic interactions-mediated lipid-based nanoparticles can be mainly divided into three subgroups: liposomes, lipo-complexes (LPCXs), and lipoplexes (LPPXs).

Liposomes (Fig. 6A(i)) refer to monolayer or multilayer nanovesicles, which are mainly composed of phospholipids. Due to their high bioavailability and biodegradability, liposomes have been considered potential nanocarriers for various therapeutic agents [130]. Even hydrophilic and lipophilic compounds will be adsorbed, and co-delivery is feasible in the same liposome system, which has greatly expanded their application ranges. The *in vivo* stability of liposomes is related to various factors, including particle size, surface charge, lipid composition, number of layers, and surface modifications like absorbed layers and grafted polymeric agents. Fabrication and surface modification of liposomes has already become one of the most popular topics in biomedical science, as the circulation stability and absorbing rate of the reticuloendothelial system of liposomes can be generally regulated by chemical methodologies.

Another noteworthy subgroup of lipid-based nanoparticles is lipo-complexes (also known as lipid nanoparticles, LPCXs) (Fig. 6A(ii)), which are widely used for nucleic acid delivery [131]. The main difference between LPCXs and liposomes is that LPCXs form condensed structures with polymers and therapeutic agents, and the morphology of LPCXs can be changed by shifting the synthesis formula and fabrication parameters. The simple fabrication processes, low biotoxicity, and notable serum stability have indicated the high potential of LPCXs in personalized, precise therapy. However, despite these advantages of the LPCX system, applications are still limited due to the high uptake of the liver and spleen, as well

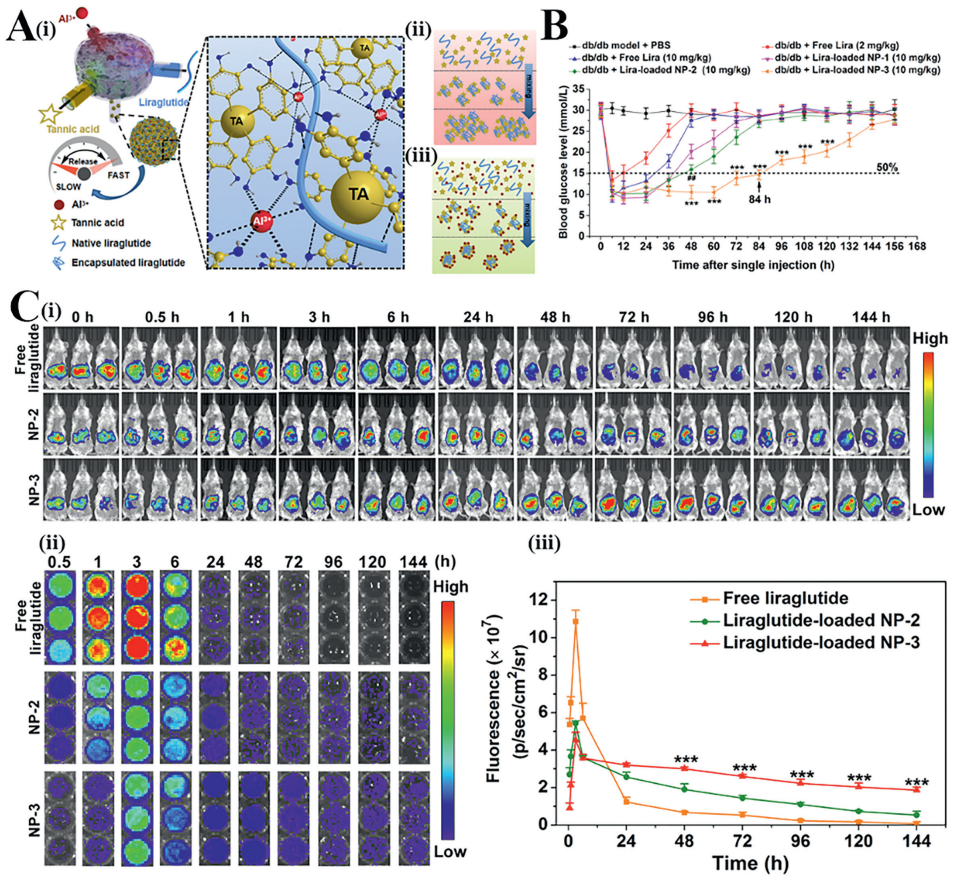

Fig. 5. (A) (i) FNC devices for nanoparticle formulation and the inner complex structure of the ternary network; (ii) illustration of the aggregation of Lira/TA complexes without Al^{3+}; (iii) illustration of the nanoparticle formation of the ternary nanoparticles with Al^{3+}. (B) Blood glucose levels (BGL) of *db*/*db* mice following a single *i.p.* injection of free Lira or Lira-loaded nanoparticles. (C) (i) *In vivo* fluorescence imaging of the mice upon *i.p.* injections of Cy7.5-labelled free Lira and Lira-loaded nanoparticles at different time points; (ii) fluorescence imaging of blood samples collected at different time points; (iii) semi-quantification of fluorescence intensity of the Cy 7.5-labelled Lira in blood samples. Copied with permission [122]. Copyright 2020, Elsevier.

as the low drug loading efficiency and poor specific biological distribution of LPCXs.

Lipoplexes (also known as lipo-polyplexes, LPPXs) (Fig. 6A(iii)) were derived and developed from traditional LNPs by covering a polymer-drug complex core with a lipid shell to form a stable core-shell structure [132,133]. The lipid shell can enhance the bioavailability of LPPXs due to its high similarity with the double-layered biomembrane, which will significantly promote the endocytosis process. However, the preparation of LPPXs requires precise kinetic control of chemical reactions, which means new-generation fabrication technologies are urgently demanded.

The process of mixing lipids and other components to form lipid nanostructures can be concretized as the lattice structure of mono-component lipid aggregates is deformed when extra components are doped. Microvolume mixing technology can provide a turbulent environment and precise control of the lattice-formation dynamic, thus accelerating and optimizing the whole formulation process. Recently, research devoted to FNC-manipulated lipid-based nanoparticles has emerged and provided new perspectives on advanced lipid-based fabrication processes.

Though oral delivery is attractive as an easy and noninvasive administration route, the acidic and enzymatic gastrointestinal (GI) tract has restricted oral administrations of most biomacromolecules [134]. By applying FNC technology, He *et al.* developed a single-step strategy for fabricating lipopolyplexes and other lipid-based nanoparticles for effective oral delivery. In a four-inlet MIVM, all the flow rates at the inlets were programmed to be equal, and by changing the types of components and solvents in the stream, continuous production of various nanoparticles was promoted. In the process of manufacturing LPXs, 1,2-dipalmitoyl-*sn*-glycero-3-phosphocholine (DPPC) and cholesterol participated in the fabrication of the lipid shell, along with *l*PEI and pDNA participating in the fabrication of the polymeric-complexed core. At the injection rate of 30 mL/min, batches of scale-up nanoparticles from 5 mL to 200 mL are fabricated and purified by tangential flow filtration (TFF) (Fig. 6B). The size distributions of all nanoparticles at different batch scales were nearly identical, proving the high consistency of the TFF-coupled FNC system. Compared with traditional formulation methods, including rapid injection and thin-film methods, nanoparticles fabricated by the FNC-TFF system have optimized size distribution and relatively smaller particle size (~70 nm) (Fig. 6C). Moreover, according to the result of long-time imaging of bioluminescence, *in vivo* experiments exhibited appreciable transgene expression target organs upon the dosage of LPXs, proving the high organ-targeting ability and high capability of the lipid shell structure protecting the polymeric-complex core against the environment of the GI track (Fig. 6D). By combining FNC devices with advanced filtration devices, continuous processing with expandible scalability to prepare high-efficiency DNA-containing nanocarriers has been accomplished [134].

Based on the research mentioned above, Nie *et al.* adapted the FNC-TFF system in fabricating insulin gene-loaded lipopolyplexes [135]. As the positively charged lipid will strongly interact with the mucosa, 1,2-dimyristoyl-rac-glycero-3-methoxy poly(ethylene glycol)-2000 (DMG-PEG) was used, as the grafting of PEG will significantly decrease the surface charge and thus enhance the mucus

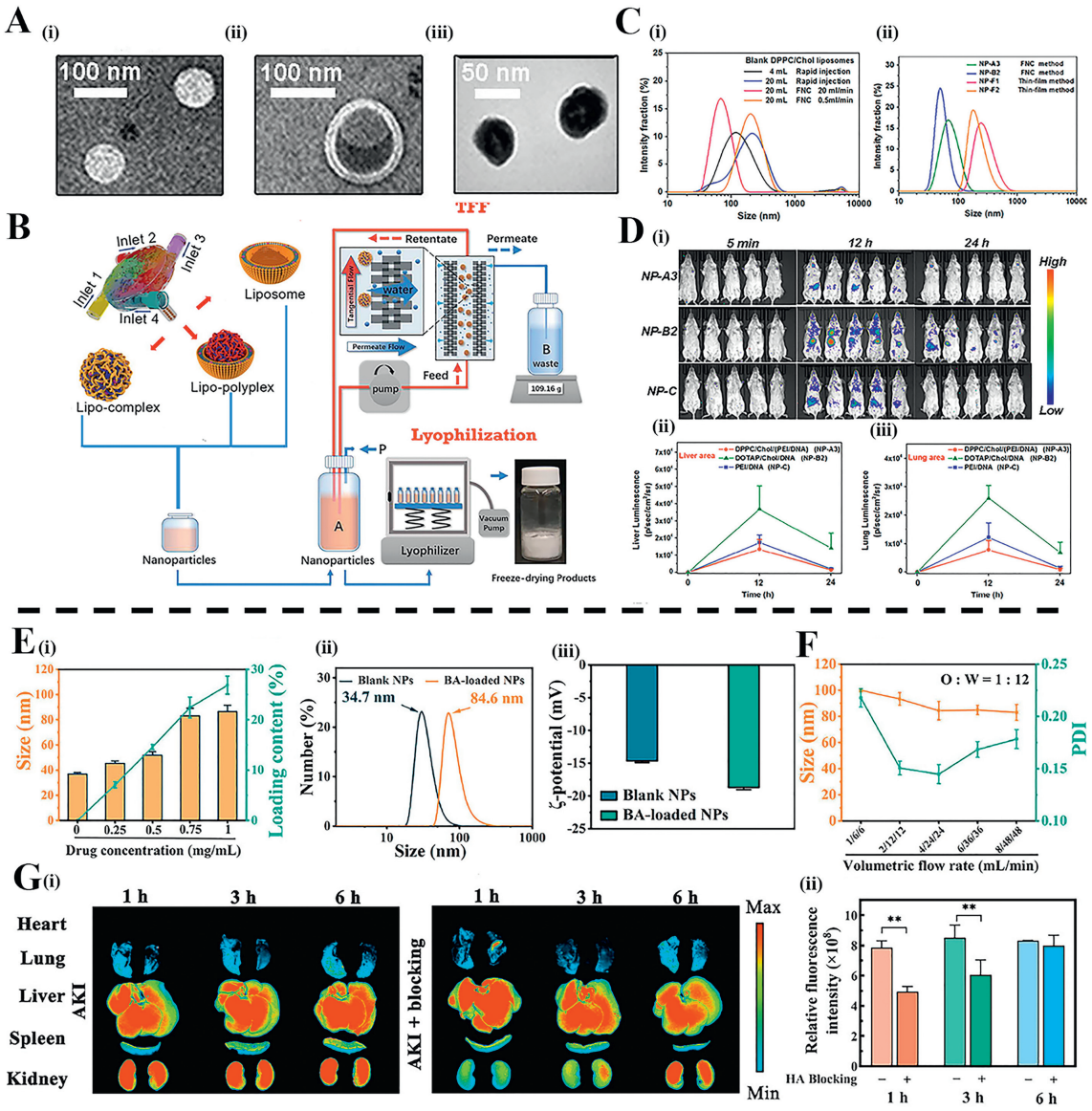

Fig. 6. (A) Structure and TEM images of different lipid-based nanocarriers. (i) Liposomes; (ii) lipid nanoparticles; (iii) lipoplexes. (B) Schematic diagram of the continuous fabrication and purification of various nanoparticles by combining FNC and TFF devices. (C) Size distribution of different nanoparticles *via* FNC and traditional methods. (i) Blank DPPC/Chol liposomes generated *via* FNC and rapid injection; (ii) DPPC/Chol/PEI/DNA lipid nanoparticles prepared *via* FNC and thin-film methods. (D) Transgene expression along multiple dosages of nanoparticles. (i) Whole-body imaging of bioluminescence every 12 h with repeated dosing of nanoparticles every 24 h; semi-quantification of bioluminescence signal in the liver (ii) and lung (iii) over time. Copied with permission [134]. Copyright 2018, Elsevier. (E) (i) Effects of BAPTA-AM concentration on particle size and drug loading content; (ii) size distribution of blank nanoparticles and nanoparticles loaded with BAPTA-AM. (iii) ζ-potential of blank nanoparticles and nanoparticles loaded with BAPTA-AM. (F) Effects of flow rate on the size distribution of BAPTA-AM-loaded nanoparticles when the ratio between the organic phase and aqueous phase was fixed at 1:12. (G) (i) *Ex vivo* images of major organs in AKI rats or CD44-blocking AKI rats; (ii) mean fluorescence intensity of the kidney. Copied with permission [140]. Copyright 2023, American Chemical Society.

permeability. With the advantages of controlled turbulent mixing and assembly kinetics of FNC, batches of morphology uniformed lipo-polyplexes loading insulin genes were fabricated, and the results of immunohistochemical analysis proved that this strategy of doping PEGylated lipid into the formation of DNA/LPXs have the potential to serve as a simple and effective method for oral delivery [135].

Besides amphiphilic lipid molecules, grafting heterophilic blocks on macromolecular backbones to form amphiphilic molecules is another commonly used strategy for forming micelles and nanoparticles for drug delivery [136–138]. When the grafted polymer is dispersed in an aqueous solution, self-assembly occurs to form nanocarriers with core-shell or condensed nanostructures. After encapsulating the hydrophobic molecules, the micelles or nanoparticles can still maintain relatively higher water dispersibility. This strategy has attracted enormous attention for fabricating nanoformulations for the delivery of therapeutic agents with poor water solubility [139].

Target delivery of calcium chelators has been proven to be a valid strategy for repressing calcium overload, which is considered a determinate cellular event of acute liver or kidney injury. 1,2-Bis(2-aminophenoxy)ethane–*N*,*N*,*N*′,*N*′–tetraacetic acid acetoxymethyl ester (BAPTA-AM) is a calcium chelator prodrug with high ionic selectivity and biomembrane permeability. However, the poor water solubility of BAPTA-AM severely limited its *in vivo* stability and thus hampered further applications. Recently, based on the binding ability between hyaluronic acid (HA) and CD44 receptors (an overexpressed receptor protein in in-

jured kidneys), Wang *et al.* designed a drug delivery platform by binding hydrophobic antioxidant bilirubin (Br) and HA with adipic dihydride (ADH) linkers to form the grafted polymer HA-Br with both amphipathic and ROS responsiveness [140]. By using the FNC strategy, hydrophilic-hydrophobic interaction-induced self-assembly processes of BAPTA-AM-encapsulated nanoparticles were yielded with high efficiency and reproducibility under precise kinetic control. While increasing the concentration of BAPTA-AM to 1 mg/mL and HA-Br to 2 mg/mL, both the encapsulation efficiency and loading content were increased, but the colloidal stability was decreased (Fig. 6E). Moreover, flow rates of impinging flow in the CIJ mixer of FNC acted as an essential factor in the self-assembly process when multiple components were employed in the turbulent environment. In the process of fabricating HA-Br nanoparticles, when flow rates were increased under a certain value (total flow rate at 52 mL/min), as the diffusion distance was reduced, nanoparticles with a narrower size distribution were produced (PDI = 0.14, decreased from 0.23 when the total flow rate was at 13 mL/min) (Fig. 6F). To evaluate the biodistribution of BA-loaded nanoparticles, *ex vivo* images of main organs were carried out for both administration groups with or without CD44 receptors blocked by HA. The obvious differences in fluorescence signals in kidneys proved that the target delivery characteristic can be attributed to the rapid accumulation of HA in the kidney and binding ability with CD44 receptors, portending greater clinical value for acute kidney injury (AKI) with an extremely narrow therapeutic window (Fig. 6G). Histological analysis of kidney sections offered the essential information that administration of HA-Br nanoparticles eliminates the AKI characteristics in tissues (*e.g.,* glomerular atrophy, interstitial edema, and cast structures in tubules). After combining with advanced nanoformulation technologies, the development of amphiphilic-polymer-based drug delivery systems has been endowed with higher feasibility to complete target delivery and a promising value for potential clinical applications [140].

6. Commercial applications of FNC technology: present and future trends

The validation of large-scale industrial production of pharmaceuticals is the last but most essential barrier for formulation technology to pass, as large-scale processing always demands tough requirements. Due to the huge disparity in material handling capacity, the difference between lab-scale processing and industrial production becomes evident. It is impossible for laboratory results to completely reflect the actual situation of industrial production as the relatively low capacity of laboratory equipment results in difficulties in fully investigating engineering factors (*e.g.,* heat transfer, mass transfer, flow, mixing) that need to be carefully considered in large-scale industrial equipment [141,142]. How to ensure the stability of industrial equipment while also maintaining high batch-to-batch reproducibility of the final products in the continuous unit operations of the industry and reducing the cost of the process at the same time has become arduous. Although the physiochemical properties of reagents and the mechanisms of chemical reactions hardly change in different production environments, the optimal reaction process conditions for every single step in the process may vary with the production scale and changeable external conditions [143,144].

Fortunately, FNC has been proven to be a powerful and stable technology that is practicable for lab-industry translation, even when facing one of the major medical crises in recent years: COVID-19. According to the website report, Pfizer/BioNTech had employed CIJ mixer and FNC technology in fabricating lipid-coated mRNA COVID-19 vaccines [145]. Compared with traditional vaccines, including nucleic acid vaccines constructed by *in vitro* transcription, mRNA vaccines present harmless small fragments of viruses to induce "dual immunity" including both humoral immunity and cellular immunity in the human body. In addition, multiple mRNAs expressing different proteins can be designed in the same preparation, which means they can be developed into "multifunctional" products. Moreover, the development cycle of mRNA vaccines is shorter than that of traditional vaccines. FNC technology is the only known method that may enable the rapid mixing of fluids while the production capacity can be enlarged to an industrial scale. The injection pumps contribute high pressure to the opposed fluidic streams to form a turbulent environment while avoiding any possible stoppages in mixers and pipe systems, which is extremely suitable for enhancing stability in industrial systems while fabricating. The highly effective production method and high colloidal stability of products also guaranteed the mRNA vaccines to overcome hazards caused by destabilization during transport [145].

The vaccine efficiency rate of Pfizer's new vaccine developed based on mRNA technology has reached about 95%, which has given the world a boost to control the epidemic [145]. Meanwhile, more mRNA vaccines against influenza, tumors, herpes, and acquired immunodeficiency syndrome (HIV) in Pfizer and its cooperative companies' pipeline are also undergoing clinical trials [145].

7. Conclusion and future perspectives

Along with the rapid development of biomedicine and drug designation, the requirement for advanced formulation technologies has become a crucial problem to be solved. Depending on the precise kinetic regulation of self-assembly processes, FNC technology has shown potential in particle size control, loading capacity, and batch-to-batch reproducibility enhancement, as well as improved biodistribution, bioavailability, and biosafety for fabricated nanoparticles. There is no doubt that FNC and its application in nanomedicine formulation and nanoparticle fabrication have made crucial progress in the clinical transition of nanomedicines as a robust and versatile strategy with better stability, which have been proven by a large number of the formulation cases shown in Table S1 (Supporting information) [82,86-88,103,104,118-123,134,140,146-161]. For future industrial applications, FNC can largely reduce the consumption of unnecessary ingredients and solvents while also enhancing the homogeneity of products and reproducibility between the same fabrication platforms in different situations. Derived and developed from the FNP method by Mao *et al.,* FNC involves electrostatic interaction and other self-assembly interactions in an aqueous system to form nanocarriers encapsulating nucleic acid, peptide, or other therapeutics in a fast and economized manner, which avoids obstructions on the way to fabricating nano-bio preparations that can be employed in bioimaging, biosensing, disease diagnosis, and treatment. However, despite the achievements mentioned above, challenges also appeared as the applications of the FNC technology were getting broader. Improvements in FNC devices and methodology are needed to satisfy further requirements.

To understand the profound mechanisms of nanoformulation and the relationship between the fabrication process and therapeutic performance, computational methods, including molecular dynamics (MD) and CFD modeling, should be brought into future studies in nanocarrier fabrication to maintain a better understanding of the mechanism in self-assembly [162,163]. Also, the industrial transition requires an enhancement in the mechanical strength and reproducibility of the devices after a thousandfold enlargement of the processing scalability. Other improvements, including optimizations in turbulent flow mixer structure, enhancements in mixer capacity, and precise regulation in numerically controlled flow systems, are also considered essential factors. Considering beyond the cost, efficiency, device stability and procedure

safety are acting as unsolved problems before turning lab-scaled FNC into industrial production [164–168].

Expanding flash technologies to cooperate with other intermolecular interactions will also improve their practicality in nanoformulations [169]. Recently, from the perspective of developing intermolecular aggregation systems with specified structures and functions, the rapid growth of supramolecular chemistry and host-guest chemistry has drawn attention from various fields in material science and molecular engineering [170–173]. On the principle of designing atomic permutations for constructing advanced intermolecular systems, supramolecular chemistry has created numerous ideas for fabricating biomaterials and nanoformulations [174–176]. As a newly emerging strategy, combining flash technologies with supramolecular chemistry might act as an important research orientation, even permanently changing the appearance of nanoformulations [177]. Mejia-Ariza *et al.* build a supramolecular interaction-promoted nanoaggregate system with β-cyclodextrin (CD)-functioned gold nanoparticles and adamantyl (Ad)-terminated poly(propyleneimine) dendrimers [178]. Systematic studies towards this nanoaggregate proved that the aggregating was driven by host-guest interactions between CD and Ad moieties, and the turbulent environment created by flash technology also played an important role in this process as a relatively short mixing time could ensure a homogeneous solvent replacement so that the properties of the nanoaggregate, especially the hydrodynamic diameter (HD), largely depend on the flow rate-ensured competitive kinetics. Higher *Re* will lead to a higher HD value, while this inclination is also related to the CD/Ad ratio, which means applying flash technology to a strongly turbulent environment can be considered a new strategy in controlling the size of host-guest interactions-driven nanoaggregates [178]. However, further study towards flash-supramolecular combination is still urgently needed at theoretical levels to help the researchers get a deeper understanding of how microvolume turbulent mixing strategies and a series of fluidic mechanic-dominated strategies can influence host-guest chemical processes [179,180].

With the continuation of efforts on systematic experimental and theoretical simulations, we can expect more effective and scalable FNC-based applications in the near future.

Declaration of competing interest

The authors declare that they have no known competing financial interests or personal relationships that could have appeared to influence the work reported in this paper.

Acknowledgments

This work was financially supported by the Sanya Yazhou Bay Science and Technology City (No. 2021JJLH0037), Taishan Scholar Foundation of Shandong Province (No. tsqn202211065), Natural Science Foundation of China (No. 82003673), Yangcheng Scholars Research Project of Guangzhou (No. 20183197), Guangzhou Science and Technology Plan (No. 201901010170).

Supplementary materials

Supplementary material associated with this article can be found, in the online version, at doi:10.1016/j.cclet.2024.109511.

References

[1] X.F. Han, Y. Lu, J.B. Xie, et al., Nat. Nanotechnol. 15 (2020) 605–614.
[2] M.W. Xiao, Z.H. Shen, W.W. Luo, et al., Biomater. Sci. 7 (2019) 4174–4185.
[3] F. Oroojalian, F. Charbgoo, M. Hashemi, et al., J. Control. Release 321 (2020) 442–462.
[4] N. Islam, V. Ferro, Nanoscale 8 (2016) 14341–14358.
[5] A.J. Clasky, J.D. Watchorn, P.Z. Chen, F.X. Gu, Acta Biomater. 122 (2020) 1–25.
[6] D.J. Drucker, Nat. Rev. Drug Discov. 19 (2020) 277–289.
[7] F. Tao, S. Ma, H. Tao, et al., Carbohydr. Polym. 251 (2021) 117063.
[8] D.J. Brayden, T.A. Hill, D.P. Fairlie, S. Maher, R.J. Mrsny, Adv. Drug Deliv. Rev. 157 (2020) 2–36.
[9] D.D. Liu, X.L. Dai, W. Zhang, et al., Biomaterials 292 (2023) 121917.
[10] P. Davoodi, L.Y. Lee, Q.X. Xu, et al., Adv. Drug Deliv. Rev. 132 (2018) 104–138.
[11] Y. Miao, T. Yang, S.X. Yang, M.Y. Yang, C.B. Mao, Nano Converg. 9 (2022) 2.
[12] M.A. Wang, Z.C. Guo, J.Y. Zeng, et al., Chin. Chem. Lett. 34 (2023) 107651.
[13] Y. Ma, K. Jiang, H.R. Chen, et al., Acta Biomater. 149 (2022) 359–372.
[14] X. Li, X. Guo, M. Hu, R. Cai, C. Chen, J. Mater. Chem. B (2023) 2063–2077.
[15] S.A. Dilliard, D.J. Siegwart, Nat. Rev. Mater. 8 (2023) 282–300.
[16] A. Chan, H.H. Wang, R.M. Haley, et al., Mol. Pharm. 19 (2022) 1104–1116.
[17] E.W. Kavanagh, J.J. Green, Adv. Healthc. Mater. 11 (2022) 2102145.
[18] A.S. Silva, J.L.D. de Tuesta, T.S. Berberich, et al., Nanoscale 14 (2022) 7220–7232.
[19] J. Cai, J. Peng, X.W. Zang, et al., Adv. Sci. 9 (2022) 2200841.
[20] N. Kumar, P. Chamoli, M. Misra, M.K. Manoj, A. Sharma, Nanoscale 14 (2022) 3987–4017.
[21] Y.J. Song, Y.Q. Huang, F. Zhou, J.S. Ding, W.H. Zhou, Chin. Chem. Lett. 33 (2022) 597–612.
[22] Y.Q. Yang, X.W. Wang, H.S. Qian, L. Cheng, Appl. Mater. Today 25 (2021) 101215.
[23] S.P. Ning, X.L. Dai, W.W. Tang, et al., Acta Biomater. 152 (2022) 562–574.
[24] M.Z. Yu, M.M. Benjamin, S. Srinivasan, et al., Adv. Drug Deliv. Rev. 130 (2018) 113–130.
[25] B.K. Lee, Y. Yun, K. Park, Adv. Drug Deliv. Rev. 107 (2016) 176–191.
[26] Y.Y. Yang, Q.L. Chen, J.Y. Lin, et al., Curr. Med. Chem. 26 (2019) 2285–2296.
[27] A.P. Singh, A. Biswas, A. Shukla, P. Maiti, Signal Transduct. Target Ther. 4 (2019) 21.
[28] L.A. Sun, X.W. Wang, F. Gong, et al., Theranostics 11 (2021) 9234–9242.
[29] D.M. Scott, R.K. Prud'homme, R.D. Priestley, Soft Matter 19 (2023) 1212–1218.
[30] H.Z. Hu, C. Yang, M.Q. Li, et al., Mater. Today 42 (2021) 99–116.
[31] Z.Y. He, Z.J. Liu, H.K. Tian, et al., Nanoscale 10 (2018) 3307–3319.
[32] M. Puccetti, A. Schoubben, S. Giovagnoli, M. Ricci, Int. J. Mol. Sci. 24 (2023) 2218.
[33] J. Li, X. Gao, Y. Wang, et al., Matter 5 (2022) 1162–1191.
[34] R. Liu, C. Luo, Z.Q. Pang, et al., Chin. Chem. Lett. 34 (2023) 107518.
[35] P. Allawadhi, V. Singh, K. Govindaraj, et al., Carbohydr. Polym. 281 (2022) 118923.
[36] F. Lussier, O. Staufer, I. Platzman, J.P. Spatz, Trends Biotechnol. 39 (2021) 445–459.
[37] H. de Waard, H.W. Frijlink, W.L.J. Hinrichs, Pharm. Res. 28 (2011) 1220–1223.
[38] P. Ebrahimnejad, A.S. Taleghani, K. Asare-Addo, A. Nokhodchi, Drug. Discov. Today 27 (2022) 471–489.
[39] J. Kim, J.D. O'Neill, N.V. Dorrello, M. Bacchetta, G. Vunjak-Novakovic, Proc. Natl. Acad. Sci. U. S. A. 112 (2015) 11530–11535.
[40] G. Hamdi, G. Ponchel, D. Duchene, J. Control. Release 55 (1998) 193–201.
[41] Z.L. Gao, X.Y. Li, K.J. Zhao, et al., Chem. Commun. 58 (2022) 7777–7780.
[42] D.F. Liu, S. Cito, Y.Z. Zhang, et al., Adv. Mater. 27 (2015) 2298–2304.
[43] A. Maged, R. Abdelbaset, A.A. Mahmoud, N.A. Elkasabgy, Drug Deliv. 29 (2022) 1549–1570.
[44] Y. Liu, G.Z. Yang, Y. Hui, S. Ranaweera, C.X. Zhao, Small 18 (2022) 2106580.
[45] P.M. Valencia, O.C. Farokhzad, R. Karnik, R. Langer, Nat. Nanotechnol. 7 (2012) 623–629.
[46] S.T. Sanjay, W. Zhou, M.W. Dou, et al., Adv. Drug Deliv. Rev. 128 (2018) 3–28.
[47] D.F. Liu, H.B. Zhang, E. Makila, et al., Biomaterials 39 (2015) 249–259.
[48] J.W. Hickey, J.L. Santos, J.M. Williford, H.Q. Mao, J. Control. Release 219 (2015) 536–547.
[49] W.S. Saad, R.K. Prud'homme, Nano Today 11 (2016) 212–227.
[50] J.M. Lim, A. Swami, L.M. Gilson, et al., ACS Nano 8 (2014) 6056–6065.
[51] Z.N. Fu, L. Li, Y.M. Wang, et al., Chem. Eng. J. 382 (2020) 122905.
[52] Y. Hao, J.H. Seo, Y. Hu, H.Q. Mao, R. Mittal, AIP Adv. 10 (2020) 045105.
[53] B.K. Johnson, R.K. Prud'homme, AIChE J. 49 (2003) 2264–2282.
[54] B. Russ, Y. Liu, R.K. Prud'homme, Chem. Eng. Commun. 197 (2010) 1068–1075.
[55] O.I. Martinez-Munoz, C.E. Mora-Huertas, Int. J. Pharm. 614 (2022) 121440.
[56] Q. He, M.M. Guo, T.Z. Jin, S.A. Arabi, D.H. Liu, Int. J. Food Microbiol. 337 (2021) 108936.
[57] B.P. Koppolu, S.G. Smith, S. Ravindranathan, et al., Biomaterials 35 (2014) 4382–4389.
[58] J. Feng, C.E. Markwalter, C. Tian, M. Armstrong, R.K. Prud'homme, J. Transl. Med. 17 (2019) 200.
[59] S. Zhang, J.J. Chen, J.L. Liu, et al., Adv. Mater. 33 (2021) 10.
[60] I.A. Hassanin, A.O. Elzoghby, Expert Opin. Drug Deliv. 17 (2020) 1437–1458.
[61] A.J. Kwiatkowski, J.M. Stewart, J.J. Cho, D. Avram, B.G. Keselowsky, Adv. Healthc. Mater. 9 (2020) 11.
[62] M. Agrawal, S. Saraf, S. Saraf, et al., J. Control. Release 327 (2020) 235–265.
[63] R.M. Lieser, D. Yur, M.O. Sullivan, W. Chen, Bioconjug. Chem. 31 (2020) 2272–2282.
[64] C.J.M. Rivas, M. Tarhini, W. Badri, et al., Int. J. Pharm. 532 (2017) 66–81.
[65] J.S. Tao, S.F. Chow, Y. Zheng, Acta. Pharm. Sin. B 9 (2019) 4–18.
[66] S.M. D'Addio, R.K. Prud'homme, Adv. Drug Deliv. Rev. 63 (2011) 417–426.
[67] C.Y. Li, Y.F. Zhang, Y.L. Wan, et al., Chin. Chem. Lett. 32 (2021) 1615–1625.
[68] J. Yang, H. Lu, M. Li, et al., Carbohydr. Polym. 178 (2017) 311–321.
[69] E. Agostini, G. Winter, J. Engert, J. Control. Release 213 (2015) 134–141.

[70] N. Chen, M.M. Johnson, M.A. Collier, et al., J. Control. Release 273 (2018) 147–159.
[71] K.M. Takeda, K. Osada, T.A. Tockary, et al., Biomacromolecules 18 (2017) 36–43.
[72] T.C.B. Klauber, R.V. Sondergaard, R.R. Sawant, V.P. Torchilin, T.L. Andresen, Acta Biomater. 35 (2016) 248–259.
[73] J.M. Williford, M.M. Archang, I. Minn, et al., ACS Biomater. Sci. Eng. 2 (2016) 567–578.
[74] Y.D. Song, C. Tang, C.H. Yin, Biomaterials 185 (2018) 117–132.
[75] N. Aibani, R. Rai, P. Patel, G. Cuddihy, E.K. Wasan, Pharmaceutics 13 (2021) 1686.
[76] C.G. Liu, Y.H. Han, R.K. Kankala, S.B. Wang, A.Z. Chen, Int. J. Nanomed. 15 (2020) 675–704.
[77] K. Park, S. Skidmore, J. Hadar, et al., J. Control. Release 304 (2019) 125–134.
[78] T.Q. Nie, Z.Y. He, Y. Zhou, et al., ACS Appl. Mater. Interfaces 11 (2019) 29593–29603.
[79] C.D.F. Lopes, N.P. Goncalves, C.P. Gomes, M.J. Saraiva, A.P. Pego, Biomaterials 121 (2017) 83–96.
[80] H.L. Xu, Q. Yao, C.F. Cai, et al., J. Control. Release 199 (2015) 84–97.
[81] J.S. Gao, S.B. Ma, X.X. Zhao, et al., Chin. Chem. Lett. 32 (2021) 3954–3961.
[82] Y. Hu, Z. He, Y. Hao, et al., ACS Nano 13 (2019) 10161–10178.
[83] M.F. Hamza, K.A.M. Salih, A.A.H. Abdel-Rahman, et al., Chem. Eng. J. 403 (2021) 19.
[84] A.W. Li, M.C. Sobral, S. Badrinath, et al., Nat. Mater. 17 (2018) 528–534.
[85] R.T. Chacko, J. Ventura, J.M. Zhuang, S. Thayumanavan, Adv. Drug Deliv. Rev. 64 (2012) 836–851.
[86] Y.Z. Hu, Y.N. Zhu, N.D. Sutherland, et al., Nano Lett. 21 (2021) 5697–5705.
[87] X. Ke, L. Shelton, Y. Hu, et al., ACS Appl. Mater. Interfaces 12 (2020) 35835–35844.
[88] X.Y. Ke, Z.H. Wei, Y. Wang, et al., Nanomed. Nanotechnol. Biol. Med. 19 (2019) 126–135.
[89] S. Zhang, E.C. Tan, R.J. Wang, et al., Nano Lett. 22 (2022) 8233–8240.
[90] X. Fu, G.Q. Zhang, Y.L. Zhang, et al., Chin. Chem. Lett. 32 (2021) 1559–1562.
[91] Y. Zhou, Y.F. Gao, L. Pang, et al., Nano Res. 16 (2022) 1042–1051.
[92] T.Q. Nie, W. Wang, X.H. Liu, et al., Biomacromolecules 22 (2021) 2299–2324.
[93] Y. Lu, A.A. Aimetti, R. Langer, Z. Gu, Nat. Rev. Mater. 2 (2017) 17.
[94] R. Vaishya, V. Khurana, S. Patel, A.K. Mitra, Expert Opin. Drug Deliv. 12 (2015) 415–440.
[95] Z.Y. Luo, Y. Deng, R.R. Zhang, et al., Colloid Surf. B 131 (2015) 73–82.
[96] F. Araujo, N. Shrestha, M.A. Shahbazi, et al., Biomaterials 35 (2014) 9199–9207.
[97] T. Vermonden, R. Censi, W.E. Hennink, Chem. Rev. 112 (2012) 2853–2888.
[98] M.J. Webber, E.A. Appel, B. Vinciguerra, et al., Proc. Natl. Acad. Sci. U. S. A. 113 (2016) 14189–14194.
[99] A. Shamloo, M. Sarmadi, Z. Aghababaie, M. Vossoughi, Int. J. Pharm. 537 (2018) 278–289.
[100] S.J. Cao, S. Xu, H.M. Wang, et al., AAPS PharmSciTech 20 (2019) 190.
[101] J. Renukuntla, A.D. Vadlapudi, A. Patel, S.H.S. Boddu, A.K. Mitra, Int. J. Pharm. 447 (2013) 75–93.
[102] S. Maher, R.J. Mrsny, D.J. Brayden, Adv. Drug Deliv. Rev. 106 (2016) 277–319.
[103] L. Sun, Z. Liu, H. Tian, et al., Biomacromolecules 20 (2019) 528–538.
[104] Z. Gui, J. Zhu, S. Ye, et al., Int. J. Pharm. 577 (2020) 119071.
[105] C.B. He, D.M. Liu, W.B. Lin, Chem. Rev. 115 (2015) 11079–11108.
[106] S.D. Huo, P.K. Zhao, Z.Y. Shi, et al., Nat. Chem. 13 (2021) 131–139.
[107] K.A. Soliman, K. Ullah, A. Shah, D.S. Jones, T.R.R. Singh, Drug Discov. Today 24 (2019) 1575–1586.
[108] A.M. Vargason, A.C. Anselmo, S. Mitragotri, Nat. Biomed. Eng. 5 (2021) 951–967.
[109] C.R. Wan, L. Muya, V. Kansara, T.A. Ciulla, Pharmaceutics 13 (2021) 288.
[110] E.J. Carbone, T. Jiang, C. Nelson, N. Henry, K.W.H. Lo, Nanomed. Nanotechnol. Biol. Med. 10 (2014) 1691–1699.
[111] S. Van Herck, B.G. De Geest, Acta Pharmacol. Sin. 41 (2020) 881–894.
[112] J.J. Zou, G.H. Wei, C.X. Xiong, et al., Sci. Adv. 8 (2022) eabm4677.
[113] F.F. An, X.H. Zhang, Theranostics 7 (2017) 3667–3689.
[114] M. Vedhanayagam, M. Nidhin, N. Duraipandy, et al., Int. J. Biol. Macromol. 99 (2017) 655–664.
[115] H. Mao, J.L. Santos, Y. Ren, J. Williford, Patent, US2020101023A1, 2019.
[116] Y.T. Zhao, L. Liu, Y. Zhao, Z.Y. Xie, J. Neurol. 269 (2022) 1834–1850.
[117] J. Margolesky, C. Singer, Ther. Adv. Neurol. Disord. 11 (2018), doi:10.1177/1756285617737728.
[118] T. Nie, Z. He, J. Zhu, et al., Nano Res. 14 (2021) 2749–2761.
[119] Z.C. Le, Z.J. Liu, L.L. Sun, L.X. Liu, Y.M. Chen, ACS Appl. Bio Mater. 3 (2020) 5202–5212.
[120] Z. Liu, Z. Le, L. Lu, et al., Nanoscale 11 (2019) 9410–9421.
[121] Y.A. Wang, X.Y. Song, L.W. Zhuang, et al., Int. J. Pharm. 611 (2022) 121317.
[122] Z.Y. He, T.Q. Nie, Y.Z. Hu, et al., J. Control. Release 318 (2020) 86–97.
[123] D. Wang, T.Q. Nie, C.Q. Huang, et al., Small 18 (2022) 2203227.
[124] Lipid nanoparticle drug delivery, Nat. Biotech. 40 (2022) 1326.
[125] M.J. Mitchell, M.M. Billingsley, R.M. Haley, et al., Nat. Rev. Drug Discov. 20 (2021) 101–124.
[126] P. Gershkovich, K.M. Wasan, C.A. Barta, Crit. Rev. Ther. Drug 25 (2008) 545–584.
[127] H.L. Mu, R. Holm, A. Mullertz, Int. J. Pharm. 453 (2013) 215–224.
[128] N. Thomas, R. Holm, T. Rades, A. Mullertz, AAPS J. 14 (2012) 860–871.
[129] K.T. Magar, G.F. Boafo, X.T. Li, Z.J. Chen, W. He, Chin. Chem. Lett. 33 (2022) 587–596.
[130] T.M. Allen, P.R. Cullis, Adv. Drug Deliv. Rev. 65 (2013) 36–48.
[131] V. Mishra, K.K. Bansal, A. Verma, et al., Pharmaceutics 10 (2018) 191.
[132] C.T. de Ilarduya, N. Duzgunes, Expert Opin. Drug Deliv. 10 (2013) 1583–1591.
[133] S. Luozhong, Z.F. Yuan, T. Sarmiento, et al., Nano Lett. 22 (2022) 8304–8311.
[134] Z.Y. He, Y.Z. Hu, T.Q. Nie, et al., Acta Biomater 81 (2018) 195–207.
[135] T.Q. Nie, Z.Y. He, J.C. Zhu, L.X. Liu, Y.M. Chen, Adv. Therap. 3 (2020) 2000016.
[136] N.M. Hamelmann, S. Uijttewaal, S.D. Hujaya, J.M.J. Paulusse, Biomacromolecules 23 (2022) 5036–5042.
[137] K. Bruggeman, M. Zhang, N. Malagutti, et al., ACS Appl. Mater. Interfaces 14 (2022) 12068–12076.
[138] Z.H. Guo, L.Q. Shi, H.Y. Feng, et al., Chin. Chem. Lett. 32 (2021) 1046–1050.
[139] J.J. Li, J.J. Wei, Y.X. Gao, et al., Chin. Chem. Lett. 34 (2023) 107662.
[140] Y.A. Wang, M.J. Pu, J.H. Yan, et al., ACS Nano 17 (2023) 472–491.
[141] G. Chiarappa, M. Grassi, M. Abrami, et al., Curr. Drug. Deliv. 14 (2017) 158–178.
[142] B.R. Bakshi, Annu. Rev. Chem. Biomol. 10 (2019) 265–288.
[143] N.C. Neyt, D.L. Riley, React. Chem. Eng. 6 (2021) 1295–1326.
[144] J. Riese, M. Grunewald, Chem. Ing. Tech. 92 (2020) 1887–1897.
[145] Cable News Network, Pfizer Vaccine: How one company makes its millions of Covid-19 vaccine doses, 2021. https://edition.cnn.com/2021/03/31/health/pfizer-vaccine-manufacturing/index.html.
[146] Y.Z. Hu, H.W. Liu, I. Minn, M. Pomper, H.Q. Mao, Mol. Ther. 26 (2018) 168.
[147] J.L. Santos, Y. Ren, J. Vandermark, et al., Small 12 (2016) 6214–6222.
[148] H.W. Liu, Y.Z. Hu, Y. Ren, et al., ACS Appl. Mater. Interfaces 13 (2021) 30326–30336.
[149] Z.W. Xia, Z.N. Fu, L. Li, et al., Polymers 14 (2022) 2133.
[150] H.Z. Hu, C. Yang, F. Zhang, et al., Adv. Sci. 8 (2021) 2002020.
[151] X.Y. Ke, H.Y. Tang, H.Q. Mao, Int. J. Pharmaceut. 564 (2019) 273–280.
[152] D.D. Qiao, L.Y. Li, L.X. Liu, Y.M. Chen, ACS Appl. Mater. Interfaces 14 (2022) 50592–50600.
[153] S.P. Miguel, J. Loureiro, M.P. Ribeiro, P. Coutinho, Int. J. Biol. Macromol. 204 (2022) 9–18.
[154] D.D. Qiao, Y.M. Chen, L.X. Liu, Biomaterials 269 (2021) 120674.
[155] Z.Y. He, J.L. Santos, H.K. Tian, et al., Biomaterials 130 (2017) 28–41.
[156] H.K. Tian, Z.Y. He, C.X. Sun, et al., Adv. Healthc. Mater. 7 (2018) 1800285.
[157] L.L. Sun, Z.C. Le, S.R. He, et al., Mol. Pharmaceutics 17 (2020) 757–768.
[158] L. Li, Y.C. Zhang, Y. Zhou, et al., Hepatology 76 (2022) 1660–1672.
[159] T.Q. Nie, H.Y. Liu, Z.W. Fang, et al., ACS Nano 17 (2023) 10925–10937.
[160] T.Q. Nie, Z.W. Fang, H.Y. Liu, et al., Chem. Eng. J. 446 (2022) 137353.
[161] Z.Y. He, Y.Z. Hu, Z.Z. Gui, et al., J. Control. Release 301 (2019) 119–128.
[162] R. Maleki, S. Rezvantalab, M.A. Shahbazi, Nanomedicine 16 (2021) 2133–2136.
[163] M. Shamsi, A. Mohammadi, M.K.D. Manshadi, A. Sanati-Nezhad, J. Control. Release 307 (2019) 150–165.
[164] S. Bhatnagar, K. Dave, V.V.K. Venuganti, J. Control. Release 260 (2017) 164–182.
[165] H. Cho, S. Kumar, D. Yang, et al., ACS Sens. 3 (2018) 65–71.
[166] O. Veiseh, B.C. Tang, K.A. Whitehead, D.G. Anderson, R. Langer, Nat. Rev. Drug Discov. 14 (2015) 45–57.
[167] A. Watermann, J. Brieger, Nanomaterials 7 (2017) 17.
[168] R. Zaman, R.A. Islam, N. Ibnat, et al., J. Control. Release 301 (2019) 176–189.
[169] U. Chintapula, S. Yang, T. Nguyen, et al., ACS Appl. Mater. Interfaces 14 (2022) 56498–56509.
[170] Q.D. Hu, G.P. Tang, P.K. Chu, Acc. Chem. Res. 47 (2014) 2017–2025.
[171] N. Basilio, U. Pischel, Chem. Eur. J. 22 (2016) 15208–15211.
[172] L.X. Xu, R.R. Wang, W. Cui, et al., Chem. Commun. 54 (2018) 9274–9277.
[173] D. Jeong, S.W. Joo, V.V. Shinde, E. Cho, S. Jung, Molecules 22 (2017) 1311.
[174] S. Bernhard, M.W. Tibbitt, Adv. Drug Deliv. Rev. 171 (2021) 240–256.
[175] M.J. Webber, R. Langer, Chem. Soc. Rev. 46 (2017) 6600–6620.
[176] R.J. Dong, Y.F. Zhou, X.H. Huang, et al., Adv. Mater. 27 (2015) 498–526.
[177] S.K. Li, Y. Gao, Y.F. Ding, A.N. Xu, H.P. Tan, Chin. Chem. Lett. 32 (2021) 313–318.
[178] R. Mejia-Ariza, J. Huskens, J. Mat. Chem. B 2 (2014) 210–216.
[179] D. Cheng, S. Theivendran, J. Tang, et al., J. Colloid Interface Sci. 628 (2022) 297–305.
[180] J.H. Zuo, X. Gao, J.R. Xiao, Y.Y. Cheng, Chin. Chem. Lett. 34 (2023) 107827.